APPLIED AERODYNAMICS Of WIND POWER MACHINES

Robert E. Wilson And Peter B. S. Lissaman

Supported by the National Science Foundation,
Research Applied to National Needs (RANN)
Under Grant No. GI-418340

Oregon State University

MAY 1974

APPLIED AERODYNAMICS

OF

WIND POWER MACHINES

by

Robert E. Wilson
Oregon State University
Corvallis, Oregon 97331

and

Peter B. S. Lissaman
Aerovironment, Inc.
Pasadena, California

July, 1974

TABLE OF CONTENTS

Table of Contents (cont'd.) page

LIST OF FIGURES

List of Figures (cont'd.) page

LIST OF TABLES

APPLIED AERODYNAMICS OF WIND MACHINES

CHAPTER 1

INTRODUCTION

Recent interest in wind machines has resulted in the reinvention and analysis of many of the wind power machines developed over the past centuries. Because of the considerable time period since the last large scale interest in this country, which occurred over twenty-five years ago (1) a considerable amount of information that was published is out of print or not generally available. An excellent bibliography of the work published prior to 1945 was collected by the War Production Board in a report issued by New York University (2). Golding's work (3) published in 1955 also contains an extensive bibliography and covers the work done in England in the 1950's. It is the purpose of this paper to review the aerodynamics of various types of wind power machines and to indicate advantages and disadvantages of various schemes for obtaining power from the wind.

The advent of the digital computer makes the task of preparing general performance plots for wind machines quite easy. Simple, one-dimensional models for various power producing machines are given along with their performance characteristics and presented as a function of their elementary aerodynamic and kinematic characteristics. Propeller type wind turbine theory is reviewed to level of strip theory including both induced axial and tangential velocities. It is intended that this publication be of use in rapid evaluation and comparative analysis of the aerodynamic performance of wind power machines.

1.1 Role of Aerodynamics in Wind Power

The success of wind power as an alternate energy sources is obviously a direct function of the economics of production of wind power machines. In this regard, the role of improved power output through the development of better aerodynamic performance offers some potential return, however, the focus is on the cost of the entire system of which, the air-to-mechanical-energy transducer is but one part. The technology and methodology used to develop present day fixed and rotating-wing aircraft appears to be adequate to develop wind power.

One of the key areas associated with future development of wind power is rotor dynamics. The interaction of inertial, elastic and aerodynamic forces will have a direct bearing on the manufacture, life and operation of wind power systems while at the same time have a minor effect on the power output. Thus the aerodynamics of performance prediction, quasi-static in nature, is deemed adequately developed while the subject of aeroelasticity remains to be transferred from aircraft applications to wind power applications.

1.2 Wind Power Machines

Since 1920 there have been numerous attempts in designing feasible windmills for large scale power generation in accordance with modern theories. This section describes representative types of these designs.

It is convenient to classify wind-driven machines by the direction of their axis of rotation relative to wind direction as follows:

1. Wind-Axis Machines; machines whose axis of rotation is parallel to the direction of the wind.
2. Cross Wind-Axis Machines; machines whose axis or rotation is perpendicular to the direction of the wind.

CROSS-WIND-AXIS MACHINES

SAVONIUS ROTOR

The Savonius Rotor in its most simplified form appears as a vertical cylinder sliced in half from top to bottom; the two halves being displaced as shown in Figure 1.1. It appears to work on the same principle as a cup anemometer with the addition that wind can pass between the bent sheets. In this manner torque is produced by the pressure difference between the concave and convex surfaces of the half facing the wind and also by recirculation effects on the convex surface that comes backwards upwind. The Savonius design was fairly efficient, reaching a maximum of around 31%, but it was very inefficient with respect to the weight per unit power output since its construction results in all the area that is swept out being occupied by metal. A Savonius rotor requires 30 times more surface for the same power as a conventional rotor blade wind-turbine. Therefore it is only useful and economical for small power requirements.

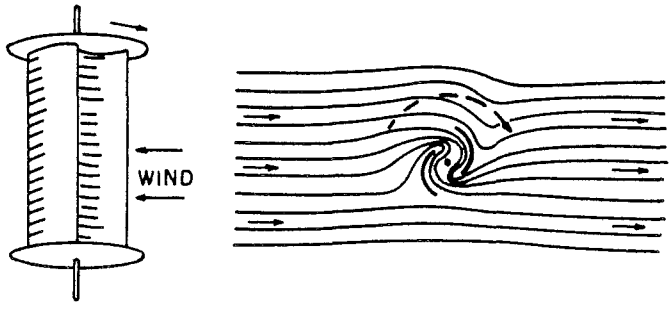

Figure 1.1 Savonius Rotor

MADARAS ROTOR

The Madaras Rotor works on the principle of the Magnus effect. In essence it involves a boundary layer control technique which attempts to suppress boundary layer formation by reduction of the relative velocity between the fluid and the solid boundary. The simplest way to achieve the Magnus effect involves the rotating of a cylinder. Figure 1.2 shows the flow pattern which exists about a rotating cylinder placed in a stream at a right angle to the flow. On the upper half of the cylinder surface, when the flow and the cylinder are moving in the same direction, separation is completely eliminated. On the lower side separation is only partly developed. Thus circulation is induced causing a lift force perpendicular to the flow and the axis of the cylinder to be produced.

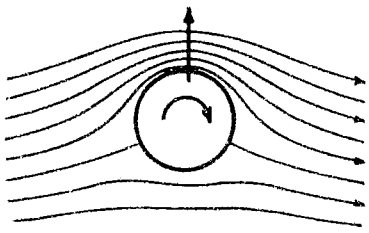

Figure 1.2 Magnus Effect

Madaras proposed to construct a circular track around which rotating cylinders, mounted vertically on flat-cars, would move. Each cylinder was to have been 90 feet high, 18 feet in diameter, and driven by an electric motor. The Magnus effect would propel the cars around the track and drive generators connected to the car axles. However the system's poor aerodynamic design, mechanical losses. and electrical losses. coupled with its unsuitability for use on mountain top locations, resulted in very little being done with this design. A single full-sized

cylinder was built in Burlington, New Jersey for testing but no further development has been done since.

DARRIEUS ROTOR

Georges Darrieus of Paris filed a United States patent in 1926 for a vertical axis rotor sketched in Figure 1.3 below.

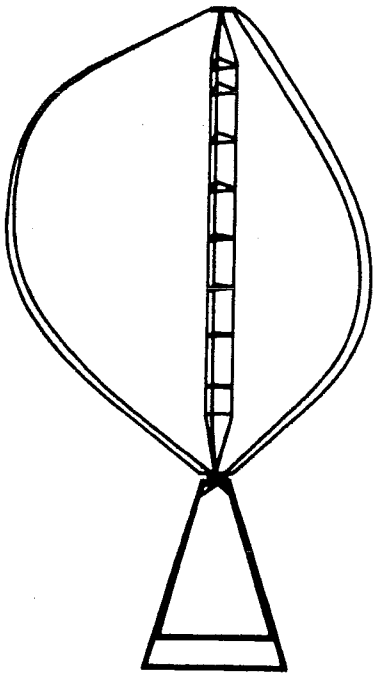

Figure 1.3 Darrieus Rotor

The Darrieus Rotor has recently been investigated by South & Rangi (20) of the National Research Council of Canada in Ottawa. The Darrieus rotor has performance near that of a propeller-type rotor and requires power input for starting. The simplicity of design and associated potential for low cost production make it a promising candidate for economical power production. The ability to scale the Darrieus type rotor to higher levels of power production, 100 kw or more, remains uncertain. To date the largest Darrieus rotors built are less than 20 feet in diameter.

WIND-AXIS MACHINES

DUCTED ROTOR

In 1954 the British built an experimental windmill with two hollow airplane-type blades as shown in Figure 1.4. Unlike conventional machines it has no coupling between the propeller and the generator. As the blades are turned by the wind, centrifugal force pulls air from the hollow tower through the blade tips. At the same time the pressure difference between the tip of the rotor and the blade pedestal also draws up air through the semi-vacuum created in the 100 foot high tower. As air flows through the tower it passes through a turbine that drives a generator. The blade was 80 feet in diameter and is capable of producing 100 kilowatts in a 35 mph wind at 95 rpm.

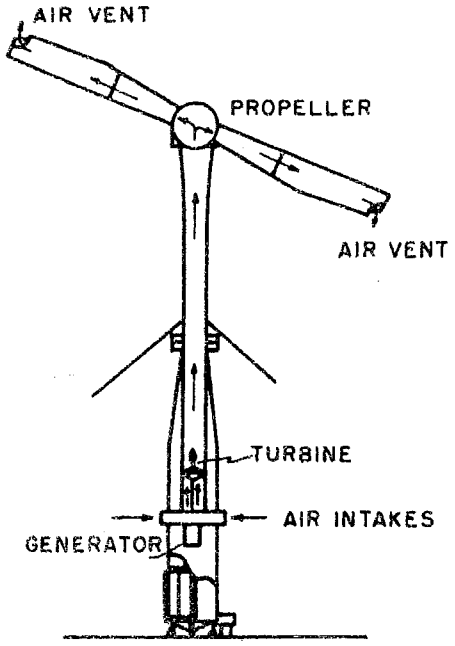

Figure 1.4 Enfield-Andreau Ducted Rotor

In order to maintain constant rotor speed hydraulic motors were used to vary the blade pitch and were effective at wind speeds of 30 to 60 mph. The blades are designed so that they

can flap under wind pressure of heavy gusts. The motion of the rotor to face into the wind is aided and controlled by a power operated system. The main advantage of this system is that the power generating equipment is not supported aloft.

SMITH-PUTNAM DESIGN

The Smith-Putnam windmill built at Grandpa's Knob in Vermont was the largest ever constructed. The rotor diameter was 175 feet and consisted of two stainless steel blades using NACA 4418 airfoil sections. The rotor and generator weighed about 250 tons and were supported by a 100 foot tower.

The pitch control was automatic, keeping the blades at a constant speed of 28.7 rpm at wind velocities of 18 mph and above. As the wind velocity increased, the blades began to feather by turning edgewise. The blades were designed with an ability to cone up to 20° to guard against sudden gusts and still maintain a reasonably constant speed. The coning was itself damped by oil-filled cylinders. The power plant was designed to withstand wind up to 120 mph and 100 mph with six inches of ice on the leading edge. The wind turbine was intended to generate 1,000 kilowatts.

The turbine, shown in Figure 1.5, was erected in 1941 and operated as a test unit until February 1943 when the 24 inch main bearing failed and a replacement could not be secured for two years. In 1945 one of the blades flew off and ended experimentation with this design.

In spite of the structural failure of the blade, the Smith-Putnam design illustrated the possibilities of electrical power generation by large scale wind turbines.

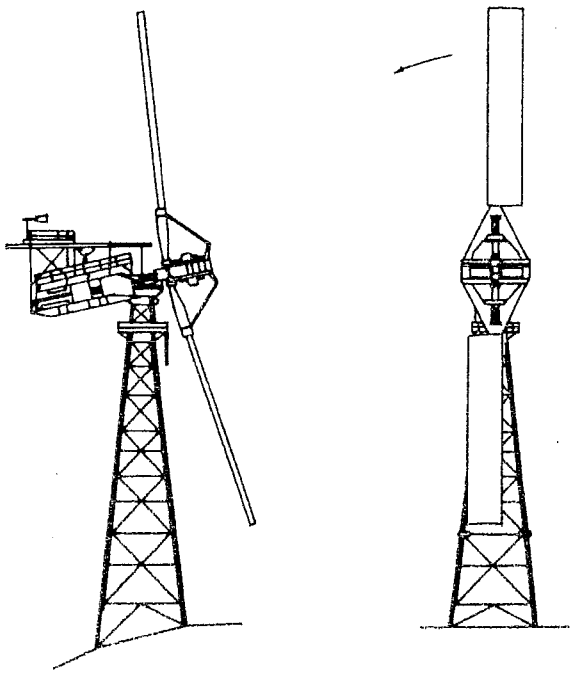

Figure 1.5 Smith-Putnam Wind Turbine

CIRCULATION-CONTROLLED ROTOR

The concept of the Circulation-Controlled Rotor Wind Turbine is quite similar to that of the Madaras Rotor and the Flettner Rotor of the 1920's. Instead of rotating the cylindrical blades of the rotor, lift is generated by blowing sheets of air tangentially around the upper surfaces of the blades from small slots. This principle, briefly, is a boundary layer control technique to delay flow separation. Blowing re-energizes the low energy boundary layer of the upper surface of the cylinder thereby moving the point of separation further back on the cylinder. Consequently, the pressure drag is reduced but there is an accompanying increase in viscous drag. At the same time circulation is induced by blowing and there is an increase in suction on the upper surface and a decrease in suction on the lower surface, all of which generate lift.

This design possesses a number of advantages. First, at zero lift the cylinder is insensitive to gusts, therefore the rotor would not tend to speed up with sudden gusts. Second, no flapping or coning is needed because the blade can be mounted rigidly to the hub without the difficulties of a conventional propeller blade that was solidly fastened. The large moment of inertia of a cylindrical cross-section of this type of blade causes it to be very stiff. The spanwise constant lift coefficient is achieved by adjusting the location of the slot, thereby foregoing complicated pitch controls. This design provides for easy construction, control, and a very rigid structure to cope with its operating environment.

An analytical investigation of this design was made at Oregon State University and it was found that at high-tip speed ratios the compressor power to drive the jet was greater than power output from the rotor, while at low-tip speed ratios the required rotor solidity (rotor projected area divided by. the disk area) was large enough to offset the structural simplicity of a circular rotor.

Figure 1.6 on the following page gives a performance comparison of the various types of rotors that have been constructed.

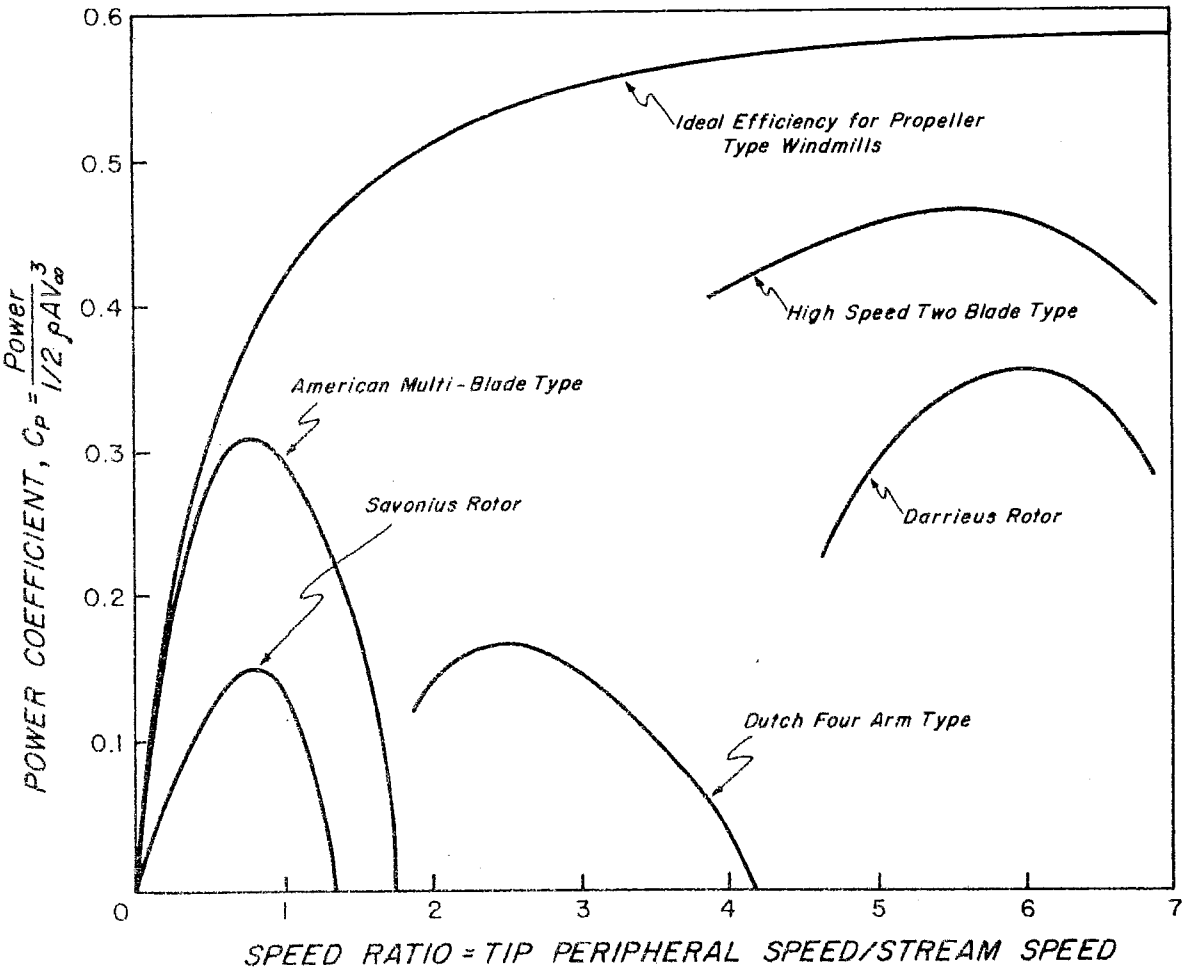

Figure 1.6 Typical Performance of Wind Power Machines.

CHAPTER 2

TRANSLATING WIND POWER MACHINES

2.1 DRAG TRANSLATORS

Perhaps the most simple type of wind power machine is the device that loves in a straight line under action of the wind.

Historically, wind-driven translating devices have been used for propulsion rather than power extraction. Analysis of translating lift-driven and drag-driven devices can be illustrative in examining various rotary machines since the translation can be considered as an instantaneous blade element of rotating machine. First, consider the machine to be driven by drag. Figure 2.1 illustrates the action of the elementary drag device.

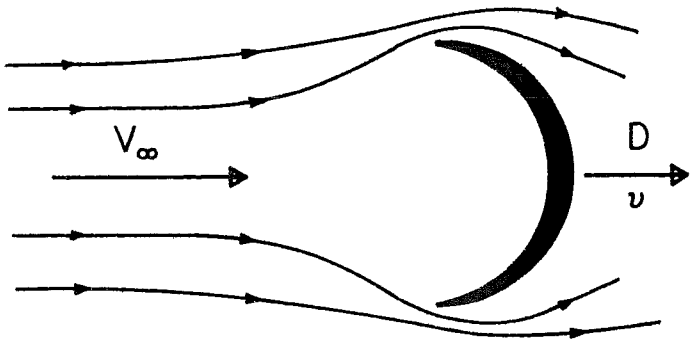

Figure 2.1 Translating Drag Device

For such a device the power extracted, P, is the product of the drag and the translation velocity. The drag device sees a relative velocity V_∞ - v so that the power is expressed by

$$P = Dv = (1/2)\rho (V_\infty - v)^2 C_D S v \qquad (2\text{-}1)$$

wind. At speeds below the wind velocity, the power output of a translator is seen to vary linearly with the translation velocity. In contrast the force produced by a translator is relatively independent of translator velocity at low speeds. The large speeds required for the translator to achieve high power extraction rates are the chief disadvantage as large speeds mean extensive capital investment in machines and land. Other disadvantages of translators are proximity to the ground and sensitivity to changes in wind direction.

CHAPTER 3

WIND AXIS ROTORS; GENERAL MOMENTUM THEORY

Now let us turn our attention to wind turbines. The propeller type windmill or wind turbine remains today, as in 1940 (1), the most efficient machine and the leading candidate for large scale wind power production. As a first step we will consider a one-dimensional analysis of the output of a wind turbine and then proceed to a more detailed approach linking blade geometry to power output.

3.1 RANKINE-FROUDE THEORY

Starting with the axial momentum theory originated by Rankine (4) and W. and R. E. Froude (5,6) consider flow past a wind turbine as shown below. The free stream wind is V_∞ which is slowed by a wind device. Applying continuity, momentum, and energy to the flow we may determine the thrust and power if the flow is assumed to be entirely axial with no rotational motion.

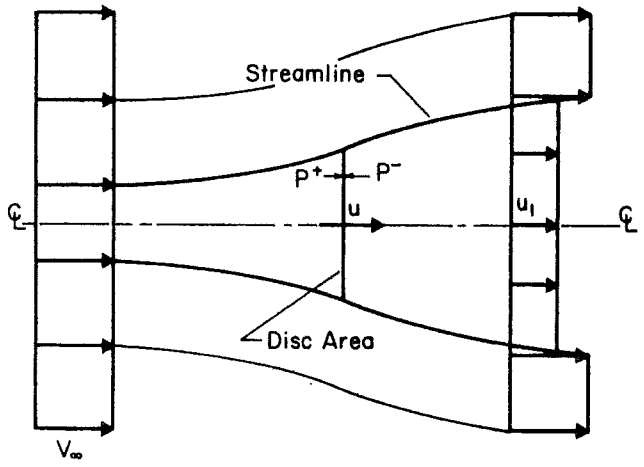

Figure 3.1 One-Dimensional Flow Past a Wind Turbine

Two expressions for the thrust may be obtained. First, from the momentum theorem

$$T = \dot{m}\left(V_\infty - u_1\right) = \rho A u \left(V_\infty - u_1\right) \tag{3-1}$$

Second from consideration of the pressure drop caused by the wind machine

$$T = A\Delta p \ , \quad \text{where} \quad \Delta p = p^+ - p^- \tag{3-2}$$

Now the Bernoulli Equation may be used between free stream and the upwind side of the turbine and again between the downwind side of the turbine and the wake so that

$$T = \rho \frac{A}{2}\left(V_\infty^2 - u_1^2\right) \tag{3-3}$$

together with the momentum expression we obtain

$$u = \frac{V_\infty + u_1}{2} \tag{3-4}$$

i.e., the velocity at the disc is the average of the initial and final velocities. If we denote $V_\infty - u \equiv aV_\infty$, note that $V_\infty - u_1 = 2aV_\infty$, the final wake velocity change $V_\infty - u_1$, is twice the velocity change at the disc. The thrust is not immediately of great importance; however, the power is. From the first law of thermodynamics, assuming isothermal flow, with $p_1 = p_\infty$

$$P = \rho A u \left\{\frac{V_\infty^2}{2} - \frac{u_1^2}{2}\right\} = \frac{\rho A u}{2}\left(V_\infty + u_1\right)\left(V_\infty - u_1\right)$$

or

$$\frac{P}{1/2\,\rho A V_\infty^3} = 4a(1-a)^2 \tag{3-5}$$

which has a maximum when a = 1/3

$$\frac{P_{max}}{1/2\,\rho A V_\infty^3} = \frac{16}{27} = 0.593 \tag{3-6}$$

Thus a maximum power is defined. The term (a) is known as the axial interference factor and is a measure of the influence of the turbine on the air. The minimum final wake velocity is zero, so as $u_1 = V_\infty (1 - 2a)$, we obtain $a_{max} = 1/2$.

When examining equation (3-6) it may be noted that the denominator is the kinetic energy of the wind contained in an area equivalent to that swept out by the rotor. Equation (3-6), however, does not represent the maximum efficiency since the mass flow rate through the disc is not AV_∞ but Au . Hence the efficiency, power output divided by power available is given by

$$\frac{P}{\rho Au\frac{V_\infty^2}{2}} = 4a(1-a) \tag{3-7}$$

The maximum efficiency is 100% at a = 1/2 which yields a power coefficient of 0.5. The efficiency at maximum power coefficient is 88.8%.

Further one-dimensional modeling can be accomplished with the additional consideration of wake rotation. As the initial stream is not rotational, interaction with a rotating wind machine will cause the wake to rotate. In the case of a propeller, the wake rotates in the direction of the propeller, in the case of an energy extracting device (windmill), the wake rotates in the opposite sense. If there is rotational kinetic energy in the wake in addition to translational kinetic energy,

then from thermodynamic considerations we may expect lower power extraction than in the case of the wake having only translation.

The following simple example will relate wake rotational kinetic energy to rotor angular velocity.

Initial Kinetic Energy $= E_{T_1}$

Power Extracted $= P$

Final Kinetic Energy $= E_{T_2} + E_{R_2}$

E_{T_2}: Translation; E_{R_2}: Rotation

From thermodynamics

$$P = E_{T_1} - E_{T_2} - E_{R_2}$$

as P = (torque) × (angular velocity), note that increased torque produces greater wake angular momentum and thereby greater wake rotational kinetic energy, so, for a given amount of initial energy E_{T_1}, the greatest power extraction will occur when E_{R_2} is low which means high angular velocity and low torque.

3.2 EFFECT OF WAKE ROTATION

Joukowski (7) considered the effect of wake rotation in the analysis of propellers. Adopting his notation to the analysis of wind turbines, the effect of wake rotation on power removal may be estimated. The wake flow model, if assumed to be irrotational, produces unrealistic rotational velocities near the rotation axis, however the contribution of the regions of high angular velocities may be subtracted out and a rotational core inserted yielding a simple model which affords utility to the results in establishing bounds.

Using a streamtube analysis, equations can be written that express the relation between the wake velocities, both axial and rotational, and the corresponding velocities at the rotor. In addition, for certain special cases, an expression for the power coefficient can be obtained. The main outcome of this approach is a measure of the effects of rotation on the relative values of the induced velocities at the rotor and in the wake.

Figure 3.2 below illustrates the streamtube.

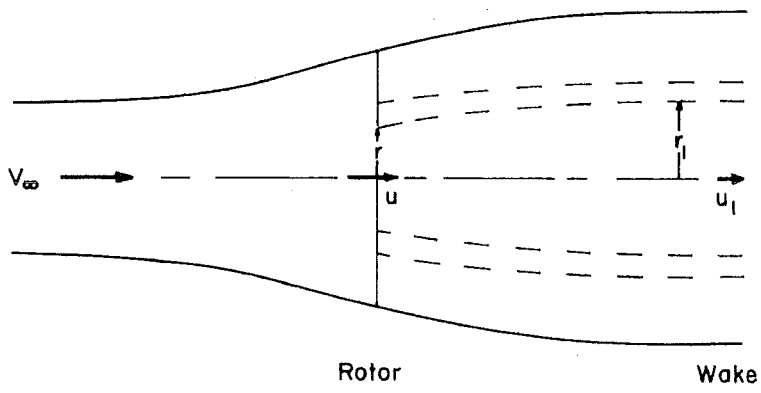

Figure 3.2 Streamtube geometry

The resulting equations are:

Continuity

$$urdr = u_1 r_1 dr \tag{3-8}$$

Moment of Momentum

$$r^2\omega = r_1^2\omega_1 \tag{3-9}$$

where ω and ω_1 are the rotor and wake angular velocities of the fluid. In addition, we may obtain an energy equation,

Energy

$$\tfrac{1}{2}(u_1 - V_\infty)^2 = \left(\frac{\Omega + \frac{\omega_1}{2}}{u_1} - \frac{\Omega + \frac{\omega}{2}}{u} \right) u_1 \omega_1 r_1^2 \tag{3-10}$$

where Ω is the angular velocity of the rotor. Finally an expression for the radial gradient in axial velocity may be obtained.

$$\frac{d}{dr_1}\left(\frac{V_\infty^2 - u_1^2}{2} \right) = (\Omega + \omega_1)\frac{d}{dr_1}\left(\omega_1 r_1^2\right) \tag{3-11}$$

These four equations may be used to obtain the relations between thrust, torque and flow in the wake. Closure cannot be obtained and one needs specification of one of the variables, say ω, in order to obtain a solution. The particular forms of the momentum equation used are Bernoulli's equation and Euler's equation.

Several features of the flow may be noted.

(1) The pressure varies across the wake due to the rotational velocity.

(2) The rotor and wake axial velocities vary radially.

(3) The angular velocity of the fluid, which is opposite the direction of rotation of the rotor changes discontinuously at the rotor.

(4) Fluid drag has been assumed to be zero.

Expressions for the torque and thrust for an annular element may also be obtained.

TORQUE

$$dQ = \rho u r^2 \omega dA$$

THRUST

$$dT = \rho\left(\Omega + \frac{\omega}{2}\right) r^2 \omega dA$$

From the expression for the wake radial velocity gradient, it may be seen that when $r^2\omega$ is constant the wake axial velocity is constant.

Defining

$$u_1 \equiv V_\infty(1-b)$$
$$u \equiv V_\infty(1-a)$$

We may obtain

$$a = \frac{b}{2}\left(1 - \frac{(1-a)b^2}{4X^2(b-a)}\right) \tag{3-12}$$

and

$$C_P \equiv \frac{\text{power}}{\frac{1}{2}\rho V_\infty^3 A} = \frac{b^2(1-a)^2}{b-a}$$

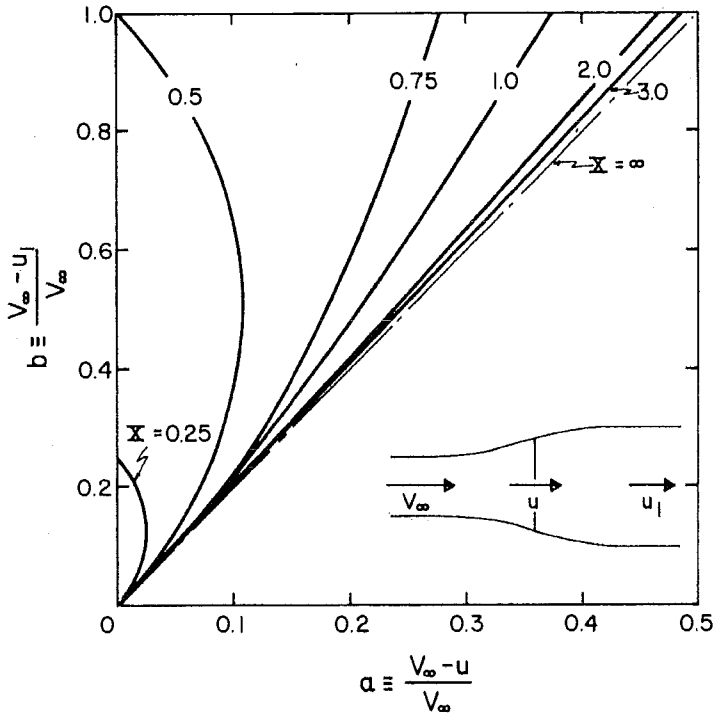

Figure 3.3 Effect of Tip Speed Ratio on the Induced Velocities for Flow with an Irrotational Wake.

Figure 3.3 above illustrates the variation of the ratio a/b as a function of a and X. It may be observed that the axial velocity change at the disc is always approximately 1/2 the value in wake for tip speed ratios above 2.

The power coefficient requires some modification since $r^2\omega$ = constant produces infinite velocities near the axis. In lieu of an irrotational vortex wake, we may substitute a Rankine vortex wake. Letting $N \equiv \Omega/\omega_{max}$, we obtain

$$C_P = \frac{b(1-a)^2}{b-a}[2Na + (1-N)b] \tag{3-13}$$

The maximum power coefficient for a rotor with a Rankine vortex wake is shown below in Figure 3.4. As would be expected the highest values of power coefficient occur at high tip speed ratios where the torque and consequently the wake rotation are the least.

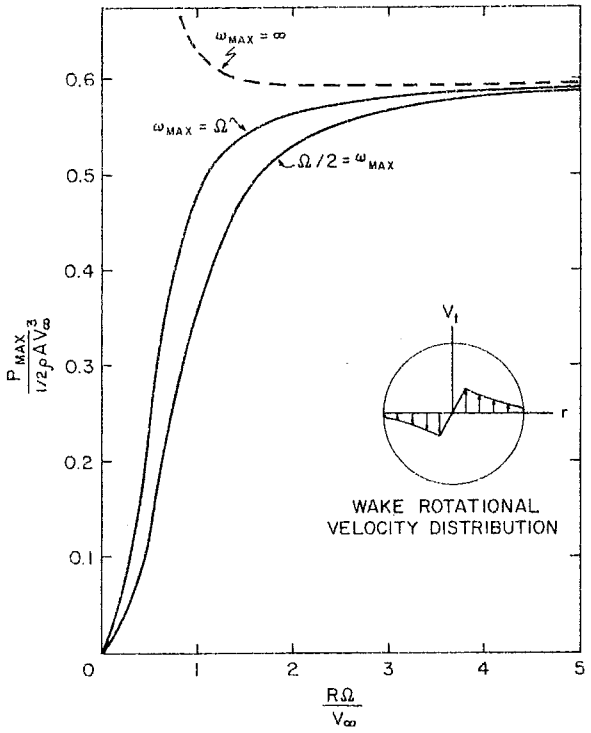

Figure 3.4 Maximum Power Coefficient vs Tip Speed Ratio for a Rotor with a Rankine Vortex Wake.

The flow model used to arrive at these results requires the flow to occur in annular, non-interacting steam tubes. Goorjian (8) has recently criticized this flow model. In spite of the difficulties associated with this model, it affords some insight into the effect of neglecting wake rotation in blade element theories of wind turbines.

3.3 SIMPLE MODEL OF MULTIPLE FLOW STATES

In the previous analysis it has been tacitly assumed that the device is operating as a draglike power extraction device, that is $0 < a < 1$. For $a < 0$ it is quite simple to continue the

analysis to show that the device will act as a propulsion producing thrust and adding energy to the wake flow. This flow regime is typical of that type of a propeller.

A particularly interesting case occurs for $a > 1$. This may be physically modeled by considering a powered propeller with its pitch adjusted so that it induces a forward flow, that is a propeller in the reverse thrust, or brake state. An idealized streamline pattern is shown below.

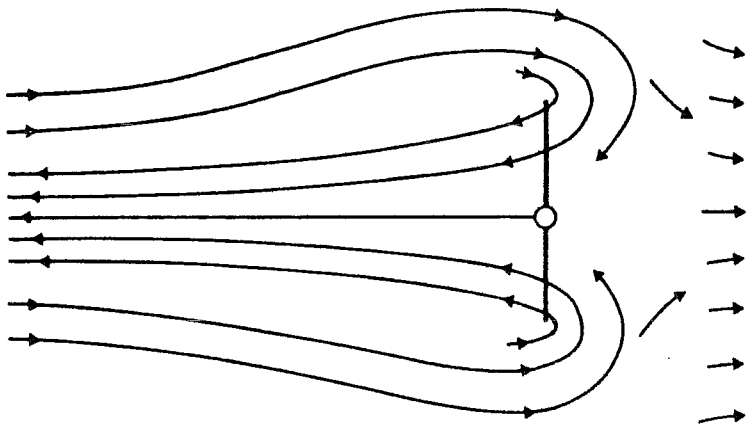

Figure 3.5 Propeller Brake State

Continuing the analysis using the same approach as in Section 3.1 we find in this case that

$$C_P = -4a(1-a)^2 \tag{3-14}$$

$$C_T \equiv \frac{\text{Force}}{\frac{1}{2}\rho A V_\infty^2} = -4a(1-a) \tag{3-15}$$

Thus, all three cases can be written in the form

$$C_T = 4a|1-a| \tag{3-16}$$

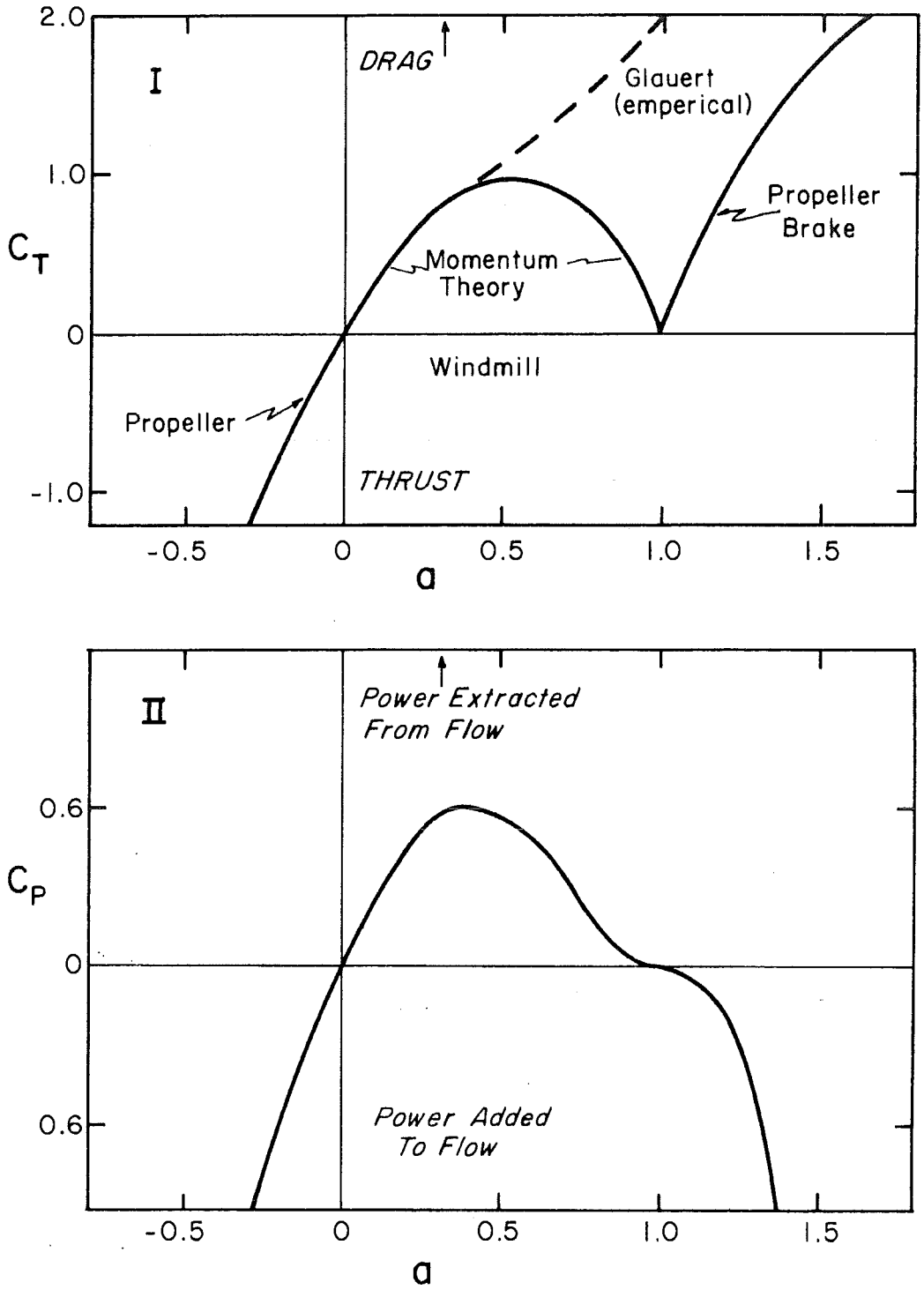

Figure 3.6 Rotor Operation Modes

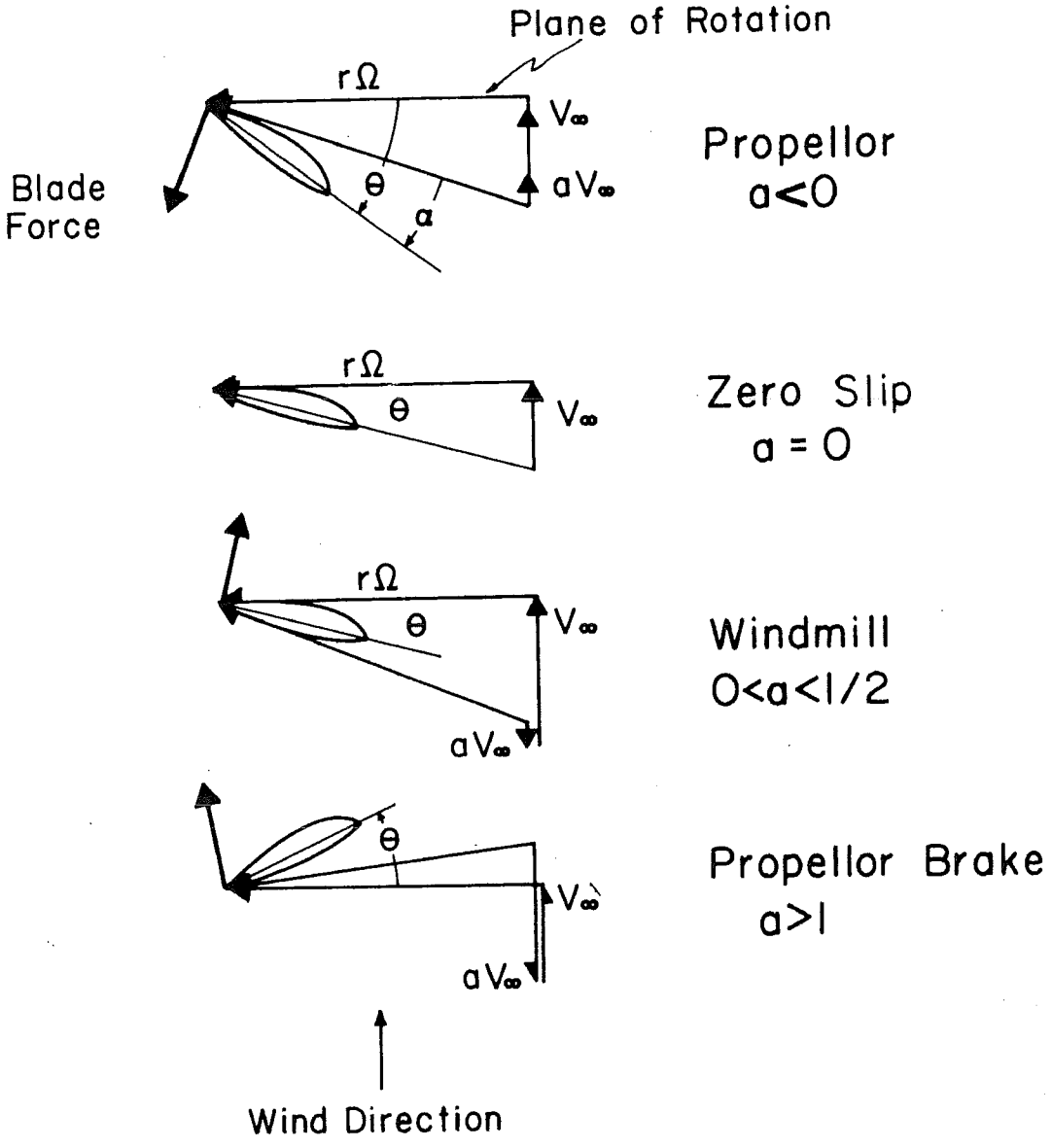

Figure 3.7 Blades Force For Various Modes

occurring at a = 1/3. It should be noted that the windmill state can still exist for $\theta = 0$; that is, for the blade to be at zero angle relative to the plane of rotation.

As θ now becomes increasingly negative, the rotor enters the propeller brake state, $a > 1$. These states are sketched in Figure 3-7, which also illustrate the sense of the force and torque on the blade. We have avoided-discussing the flow regimes in the close vicinity of a = 1 since our simplified model will break down here.

Thus, we can construct physical models of these states both by considering the flow at the disc itself and by considering the flow in the wake.

In order to establish the possibility of the modes we must connect the force as represented by wake momentum to that as represented by lifting forces on the blade elements themselves. For our simple model we will consider, as an example, the wind axis rotor (propeller) and use conventional blade element theory ignoring swirl terms and assuming the wake induced flow is twice that at the disk itself. This model is sketched in Figure 3.8.

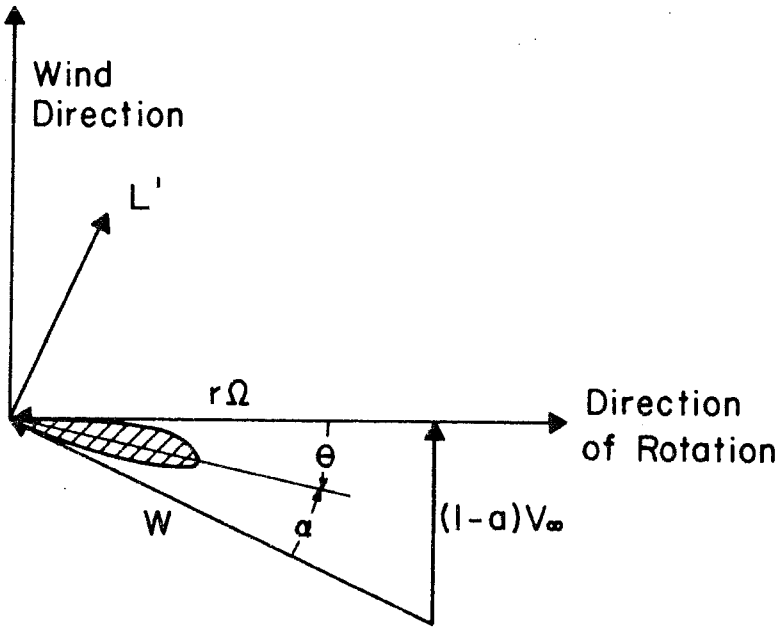

Figure 3.8 Blade Element Coordinates

Assuming we are in the propeller or windmill state $a < 1$. By momentum theory, the force on the annulus is given by

$$dT = \rho V_\infty^2 (1-a) 2a \cdot 2\pi r dr \tag{3-18}$$

and the local thrust coefficient is given by

$$C_T = 4a(1-a) \tag{3-19}$$

Now considering flow at the blade element itself we get the circulation from $\Gamma = WcC_L/2$ and with $C_L = 2\pi \sin \alpha$,

$$\Gamma = \rho \pi c \left[V_\infty (1-a) \cos \theta - \Omega r \sin \theta \right] \tag{3-20}$$

Thus the force on the annulus is given by

$$dT = \Omega r \Gamma dr \tag{3-21}$$

$$C_T = \frac{xc}{r} \left[(1-a) \cos \theta - x \sin \theta \right] \tag{3-22}$$

where x is the local tip speed ratio $r\Omega/V_\infty$.

For the propeller-brake state $a > 1$, we get by momentum theory $C_T = -4a(1 - a)$, while the blade force is given by the same result as previously. We can define a local solidity σ as $\sigma = cdr/\pi r dr$. Thus we can write for all a

$$4\pi x \sigma \left[(1-a) \cos \theta - x \sin \theta \right] = 4a \left| 1-a \right| \tag{3-23}$$

The nature of solutions to this equation can most easily be seen from Figure 3.9. Note that for $\theta < \theta_1$ the simple powered thrusting propeller occurs, while for $\theta < \theta_2$ the propeller brake mode occurs. The angles in the intermediate range $\theta_2 > \theta > 0$ exhibit three possible equilibrium states, two windmill modes and one propeller brake mode.

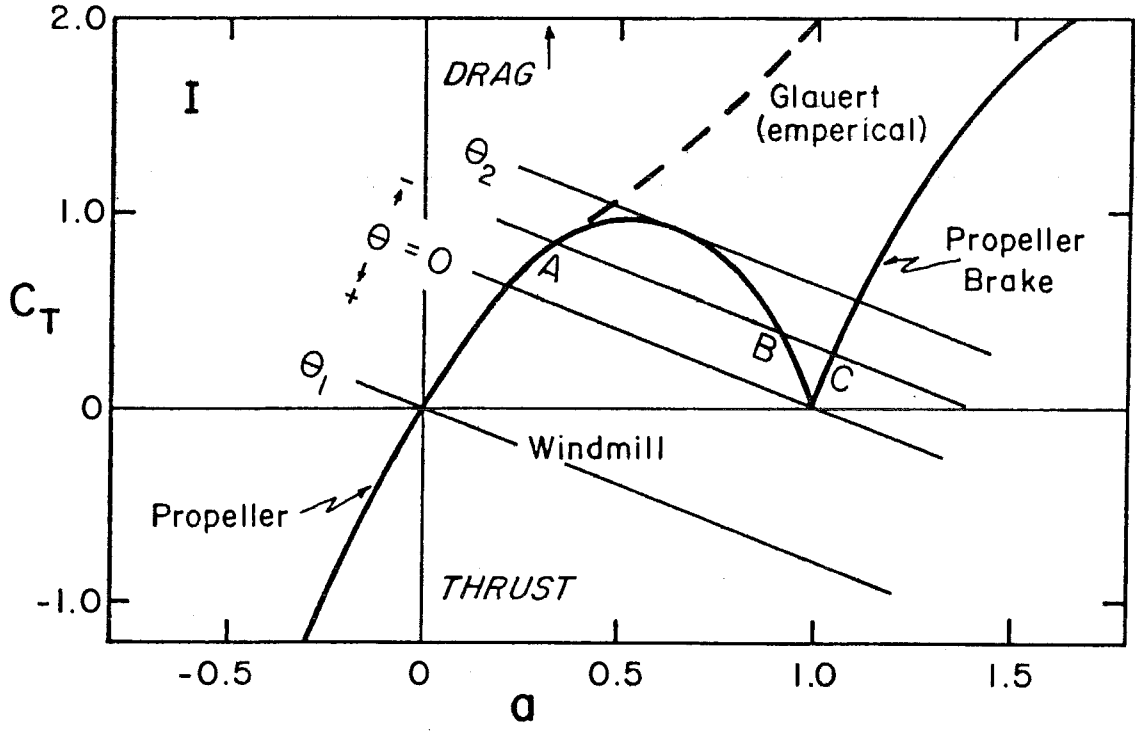

Figure 3.9 Blade Element States For Various Blade Pitch Angles.

It is of interest to note that the slope of the. blade force lines is a function of solidity and tip speed ratio.

For the triple mode case, it appears that the point shown as B is unstable and that A and C are both stable and occur depending upon how the state is approached. A simplified explanation of why state B is unstable is as fo11ows. Assume that at B, a, the induced flow is slightly increased, now the drag-force on the disk (following θ = constant) becomes much larger than

that represented by the wake momentum, thus this wake momentum is further reduced, and the system moves towards $a = 1.0$. On the other hand, A and C are stable according to these arguments. Thus a working assumption in blade element theory is that no solutions with $1/2 < a < 1$ can occur.

It should be stressed that the above is an idealized model and that it inevitably involves flow inconsistencies. For example, it can be seen that a model giving $a < 1$ on an annulus which has inner and outer annuli with the value of $a < 0.5$ will somehow violate flow continuity.

We note that states of $a > 0.5$ should not occur in the major design range of a windmill. However, in cases where it is necessary to prevent rotor over speed due to high incoming winds or reduced shaft torque loads, it may be possible to use the confused flow of the propeller brake state to dump energy. This is a method of speed control which is quite distinct from the normal blade feather technique in which a is reduced. Note that this behavior is not the same as blade stall, which occurs at the low X region of the characteristic.

We note here that the present analysis should be considered a small perturbation model, thus should not be considered valid for $a > 0.5$. For example, for $0.5 < a < 1$ the simple one-dimensional model developed here implies flow reversal in the far- wake and zero wake velocity somewhere between the actuator disc and downstream infinity, a streamline configuration which is physically unacceptable. Again the simple propeller brake analysis must be considered quite inadequate in the vicinity of $a = 1$.

No satisfactory theories exist for flow in this region, although quite extensive research has been done on this problem in connection with helicopter rotor theory. In helicopter analysis this region is that associated with a lifting descending rotor where the anomalous states of the parachute brake, the turbulent wake, and the vortex ring states occur [Shapiro, (16)].

For most normal windmill operating modes a is less than 0.5; thus it is seldom necessary to analyze conditions for a > 0.5. However, for off-design conditions spurious solutions with a > 0.5 may well occur. Rotor performance for the entire range of a is discussed by Wolkovitch (17).

It is of interest *to* note, as described by Wolkovitch, that many of the anomalies of flow near a = 1.0 can be removed by assuming that the freestream flow is not precisely axial, but yawed at some small angle to the rotor axis. The introduction of this additional degree of freedom eliminates some of the singularities which occur for axial flow. A classical approach to this problem is given by Lock, Bateman, and Townend (18).

A generalized performance curve of C_T versus a was constructed by Glauert (10) using these concepts and using data from a series of free-running windmill tests. This curve was shown in Figures 3.6 and 3.9. Since these were free running, these tests correspond to $C_P = 0$, or in helicopter terminology, the autorotative state. It should be noted that in the autorotative state one portion of the rotor is driving the remainder, thus in fact the rotor is subjected to non-uniform a, and the value of axial perturbation given is the mean a for the disc.

3.4 DUCTED ACTUATORS

Shrouds or ducts are frequently used to increase the static thrust of powered propellers. It has been well established that a duct can quite effectively reduce the slipstream contraction of a thrusting propeller and can thus increase its thrust/power ratio, at least at zero forward speed. It can be shown that, even ignoring skin friction, the effectiveness of the shroud reduces as the forward speed is increased, and when duct drag and other duct pitching moments are taken into account, the shrouded propeller is not effective technically. In calculations of ducted propeller performance it is usual to assume that the flow leaves the duct exit at freestream static pressure;

consequently, there is no further change in slipstream velocity and for purposes of calculation, the duct exit area may be taken as the ultimate wake cross section. In the case of a static free propeller, the ultimate slipstream is one half the propeller area. Thus any duct which causes the final slipstream contraction to be less than this will increase the thrust/power ratio of the system. It is of interest to observe that even a cylindrical duct of the same cross section as the propeller will increase the thrust, there will lave been no slipstream contraction. It should be noted that the increased force is represented by a forward thrust on the duct, and a major part of this contribution is the force on the leading edge and entry area of the duct due to the low pressures there.

Because of the improvement in thrusting propeller performance due to a duct, it has frequently been suggested that a ducted windmill might have superior performance. A comprehensive analysis of ducted windmills is given 'y Lilley and Rainbird (19).

From a physical viewpoint, the effect of a duct will be to increase the wake expansion. We have showed that for a free windmill the optimal wake cross section should be twice that of the windmill disc. Thus, if it is possible to cause the optimal wake cross section to be larger than this, white still keeping the wake axial induced flow at the optimal level of two thirds the free stream velocity, then, based on rotor area, the power coefficient will exceed the free rotor limit of 0.593. In effect the duct has caused more flow to be drawn through the rotor and increased its power extraction capacity. A simple analysis of this follows, in which it is shown that unlike the free rotor, a momentum type analysis cannot be made on this device without assumptions which are quite hard to justify.

In Figure 3.10 we show a typical ducted windmill system. Assuming the mass flow through the system is $\dot{m}$, we can immediately write the power extracted as

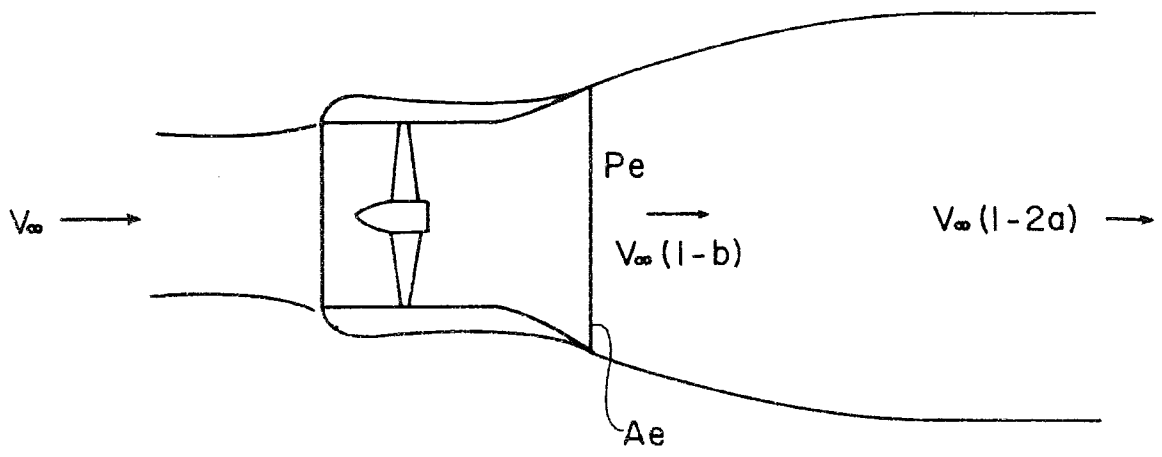

Figure 3.10 Ducted Windmill Geometry

$$P = \dot{m}\Delta H = \dot{m}V_\infty^2\ 2a(1-a) \tag{3-24}$$

This force on the entire system (rotor and duct) may be written as

$$T = \dot{m}V_\infty 2a \tag{3-25}$$

We note that these equations are not closed in that we do not have an expression for $\dot{m}$. For free actuator theory the remaining equation is readily obtained by stating that the force on the system is the force on the actuator which is given by $T = A\Delta p = A\Delta H$ where A is the actuator area. This immediately gives the result $\dot{m} = \rho AV_\infty(1 - a)$ for the free propeller case.

For our case, with the duct, it is still true that the propeller force is given by $A\Delta p$, but the duct force cannot be determined by simple momentum theory since the pressure field on the outside of the duct is not known. By one-dimensional theory the pressure on the duct interior can be calculated, except for the region very close to the leading edge. Thus, using momentum theory one additional assumption is required.

We can consider this to be satisfied by assuming the velocity at the duct exit, which is shown as $V_\infty(1 - b)$. If we assume, as is done in powered ducted propeller theory, that the pressure at the duct exit is freestream static, then we get $b = 2a$ and the mass flow can be determined as $\dot{m} = A_e \rho V_\infty(1 - 2a)$. Then, basing the power coefficient on the duct exit area A_e we obtain

$$C_P = 4a(1-a)(1-2a) \tag{3-26}$$

This expression can be maximumized to give $C_{P_{max}} = 0.385$ at $a = 0.211$. If we write power coefficient in terms of rotor area, then we get

$$C_P = 4a(1-a)(1-2a)A_e/A \tag{3-27}$$

and observe that if the duct to rotor area ratio exceed 1.54 then the power coefficient of the ducted system, based on rotor area, will exceed that of the rotor alone. At this level of analysis all performance characteristics are determined by the assumption of exit flow condition for the duct. This can be expressed by writing the power coefficient (based on exit area) and the duct exit pressure coefficient C_P^* which give us

$$C_P = 4a(1-a)(1-b) \tag{3-28}$$

$$C_P^* = -(2a-b)(2-2a-b) \tag{3-29}$$

It will be seen that, assuming the exit pressure is lower than freestream static, which must be the case, gives wake expansion downstream of the duct with a higher mass flow and higher

power coefficient. In studying Lilley and Rainbird's paper it must be noted the performance is plotted in terms of the assumed duct exit pressure.

As described in the previous sections, it is possible in principle to compute the wake shape by potential flow techniques, assuming a contour, computing internal and external flows, and ensuring pressure continuity on the wake bounding surface. Evidently the details of the duct geometry must enter into this analysis. We note that the duct cannot be treated simply as a ring wing in a uniform homoenergetic flow since the essential addition of the actuator disc implies a wake of different energy, with the associated vortex tube surrounding the wake.

Thus ducted windmills cannot be analyzed by any simple method and a proper performance prediction depends upon a modeling of the entire flow. It appears that assuming the exit pressure coefficient is a poor approximation; since the result is directly dependent on this quantity which will vary notably for every duct rotor system, and even for a given system at different rotor loadings.

CHAPTER 4

WIND AXIS ROTORS: VORTEX/STRIP THEORY

4.1 VORTEX REPRESENTATION OF THE WAKE

The wake of a windmill system consists of a flow of different total head from the mainstream. For an inviscid flow, the discontinuity in head may be represented by a sheet of vorticity. The mode of generation of this vorticity, and its geometry, can be of great assistance in developing models of the flow. In more advanced wake models we usually stipulate the wake vorticity distribution and then use the Biot-Savart Law to calculate the induced flow of this wake. It is then possible to compute the pressure and flow fields on the wake to determine whether it is in equilibrium. Thus a proper solution of the inviscid wake must involve both the kinematics and the dynamics of the flow. In other words the wake shape and strength must generally be determined by an iterative process, where the initial geometry and strength is assumed and the induced flow checked to assure the wake streamline and pressure fields are consistent. A similar situation occurs in ordinary wing theory; however, the interactive nature of the problem is usually removed by assuming the vortex wake leaves the wing parallel to the freestream flow. This implies that there will be downwash flow through the wake, a kinematically inconsistent situation. However, it is only in cases of very highly loaded wings that it is necessary to account for wake deformation.

Analogous assumptions are used for the actuator disc, where it is assumed that the wake vortex tube is parallel to the freestream flow.

If we consider the prototype actuator, a disc .which may arbitrarily be switched from zero to infinite porosity, we can create a model of the vortex ring shedding process. Assume that the

disc is oscillated forwards and backwards and is solid during the forward motion (against the mainstream) and fully porous during the rearward motion. The disc will now shed a series of ring vortices which will be convected downstream with the freestream as shown in Figure 4.1.

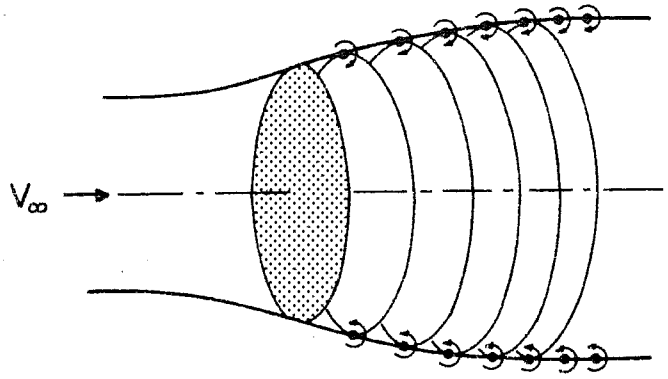

Figure 4.1 Actuator Disc

In the limit, if we assume a vortex tube of constant strength is developed, and using an hypothesis of light loads, the vortex tube will have the same diameter as the actuator disc.

Standard methods are available to compute the induced flow of a semi-infinite vortex tube at its end. We will not go into these here, except to state the solution gives a uniform induced axial flow over the cross section, although the radial flows are infinite at the tube edge. I f another vortex tube of appropriate strength were added to this system, then the singular radial flows are removed and the axial flow becomes twice that at the end of a semi-infinite tube. This is another way of demonstrating the result already obtained from the momentum analysis, that the induced flow in the downstream wake is twice that at the disc.

It will be observed that this system has no tangential velocity in the wake and hence there is no torque. For this to be an approximate model of a propeller type windmill, the tip speed ratio must be large so that for a given power the torque is in fact low.

The next refinement to add to this simple model is one which introduces torque. Consistent with actuator disc theory, we can model this with a large number of radial vorticity lines in the plane of the disc, representing a many-bladed system of constant blade circulation. In order to satisfy Helmholtz's Laws on the kinematics of vortex lines, we see that this implies a central vortex of finite strength with distributed streamwise vorticity along the wake cylinder (Figure 4.2).

A variant of this model is to assume that the actuator disc is an annulus. Then the surface of the inner vortex tube consists of ring and spanwise vortex lines of similar geometry, connected by radial vorticity at the disc itself.

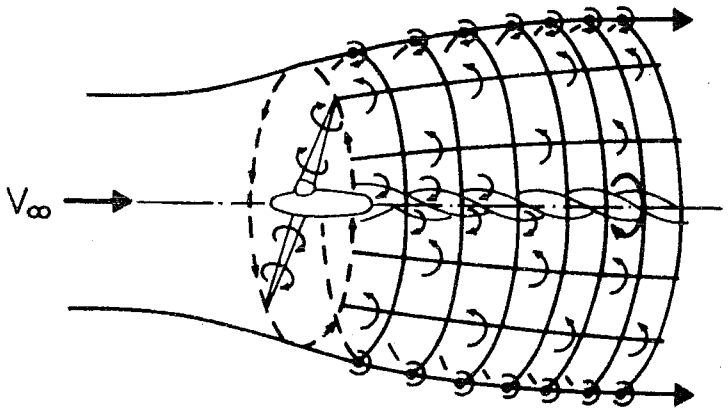

Figure 4.2 Vortex Lattice System for a Multi-Bladed Rotor (Only Two Blades Are Shown)

For a lightly loaded system in which the wake boundaries may be considered right circular cylinders parallel to the mainstream, this is a fully self-consistent model with axial and tangential perturbations entirely confined to this annular cylinder. In other words, the induced flow of such a system does not affect other annuli, as can be seen by superimposing two circular vortex tube systems. Another annulus of completely different induction could be located inside

or outside this one without affecting the induced flows in the first. Thus, the induced flow system of each annulus is a function only of the blade geometry in that annulus and the angle of attack or chord of the blade in neighboring annuli can be changed without affecting adjacent induced flows. This interesting result of annular independence is the basis of blade element theory which assumes that annuli do not interact. We note that this is different from the situation in wing theory, where changes in geometry at one spanwise station will- affect induced flows at all other stations. It is apparent that it is the idealization of continuous streamwise vorticity on the vortex wake tube which effectively isolates the induction of an annulus. Thus for non-interactive blade element theory to be valid requires that the product of the number of blades and the tip speed ratio should be large.

We note also that the concept of a continuous bounding vortex sheet composed of vortex rings permits differences in total head between the flows separated by the sheet. Thus it permits the wake flow to be of reduced total head, as assumed in simple models.

If we now consider a more realistic rotor system having a finite number of blades and rotating at a finite velocity a somewhat different situation occurs. Assuming that vortex shedding occurs only at the root and tips and that the vortex lies parallel to the local flow, then the wake vortex geometry becomes as sketched in Figure 4.3. The helix angle of the vortices is directly related to the tip-speed ratio.

We note that this finite bladed model contains somewhat similar structure to that of the wake of Figure 4.2, where the ring and streamwise vortex systems could. be considered as components of the helix system of Figure 4.3. We note also that a large tip-speed ratio, or a large number of blades will cause the finite helix sys tern to be more densely packed, so that the idealization of a continuous bounding vortex sheet becomes more realistic.

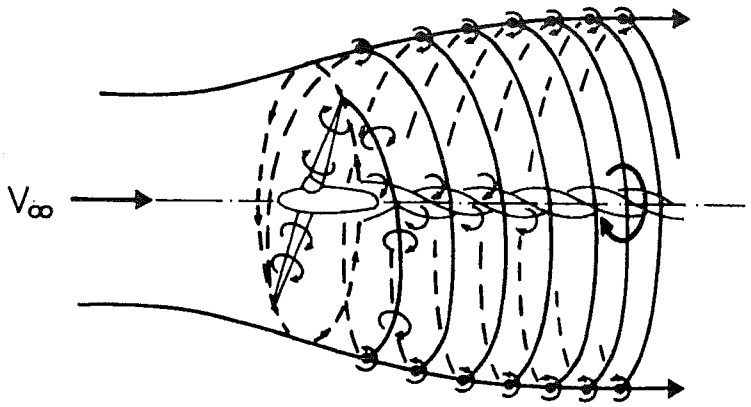

Figure 4.3 Idealization of Vortex System of a Two-Bladed Rotor

However, examination of Figure 4.3 will illustrate that near each blade the flow and vortex system is similar to that of a high aspect ratio wing. Consequently, a vortex of finite strength cannot be shed from the tips, since this would imply infinite induced washes there. Thus the local situation becomes quite similar to that of a yawing wing and a continuous sheet of vorticity is shed from the trailing edge. Generally, this vorticity is concentrated near the tip so that the idealization of a finite strength tip vortex may be quite adequate a short distance from the blade. It will be noted that for the finite bladed model there is spanwise interaction in the sense that the load on each spanwise section does influence neighboring sections so that blade element theory must be considered an approximation for a rotor with few blades at low advance ratios.

An analysis for a two-bladed rotor system at very low advance ratio is given by Kuchemann (21), where the rotor is modeled as a rolling high-aspect ratio wing.

The model in which the blades sheds a system of helical vortex sheets is generally termed the Goldstein Model. This elegant model is more complicated than most and we will not discuss it here.

4.2 ANNULUS FLOW EQUATIONS

A frequently used and accurate method for performance calculations for propellers and helicopter rotors is to assume that the flow through the rotor occurs in non-interacting circular stream tubes. This method when used in conjunction with the induced velocities has been called by a variety of names including modified blade element theory, blade element theory, vortex theory and strip theory. The method, which can be seen to assume locally 2-D flow at each radial station, proceeds as follows.

The element of a wind turbine rotor illustrated in Figure 4.4 is viewed from the tip looking towards the axis of rotation in Figure 4.5. Here the relative wind, W, is shown in relation to the local blade pitch angle θ and the local angle of attack, α. The plane of rotation is in the x-direction and the y-direction is normal to the blade in the downwind direction.

From the diagram, the following trigonometric relations may be verified

$$\alpha = \phi - \theta \tag{4-1}$$

$$\tan\phi = \frac{1-a}{1+a'}\frac{V_\infty}{r\Omega} \tag{4-2}$$

$$C_y = C_L \cos\phi + C_D \sin\phi \tag{4-3}$$

$$C_x = C_L \sin\phi - C_D \cos\phi \tag{4-4}$$

where C_L and C_D are the- sectional lift and drag coefficients based upon the local relative velocity W and the local angle of attack α.

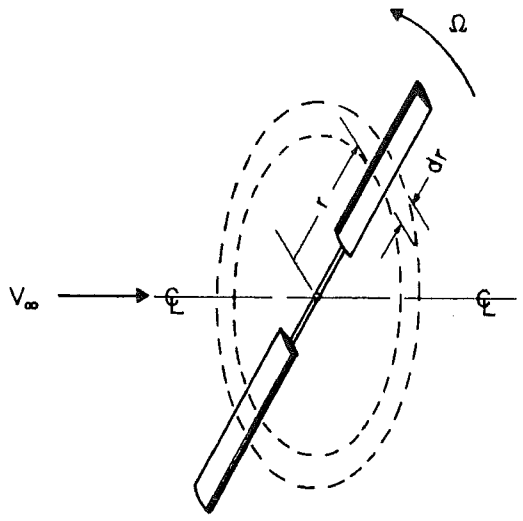

Figure 4.4 Rotor Blade Element

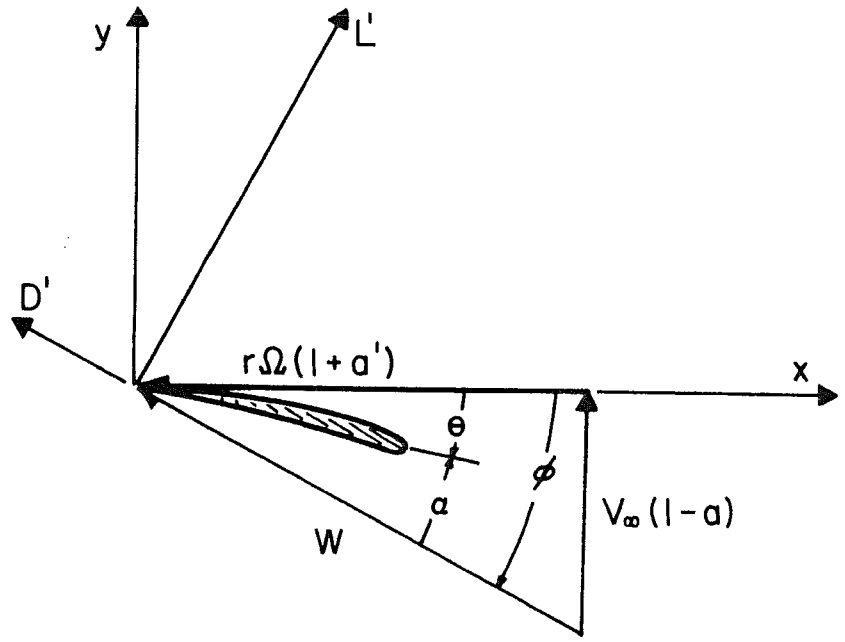

Figure 4.5 Velocity Diagram for a Rotor Blade Element

A relation between the axial interference factor a and the forces developed on the blade may be obtained by equating the axial force dT generated in an annular element of thickness dr by momentum considerations to the axial force predicted from blade element aerodynamic considerations. From momentum

$$dT_M = \rho(2\pi r dr)\, u\, (V_\infty - u_1) \tag{4-5}$$

while for B blades each having local chord c,

$$dT_B = Bc\,\tfrac{1}{2}\rho W^2 C_y dr \tag{4-6}$$

Equating these two expressions and assuming that the local wake axial interference factor b = 2a, one obtains

$$\frac{a}{1-a} = \frac{BcC_y}{8\pi r \sin^2\phi} \tag{4-7}$$

In a similar manner, the torque determined from angular momentum considerations is equated to the torque developed from the blade element in an annular differential stream tube.

From the moment of momentum theorem one obtains

$$dQ = \rho(2\pi r dr) ur\,(2a'\Omega) \tag{4-8}$$

where the angular velocity imparted to the slip stream has been assumed to be twice the angular velocity at the rotor disk. The blade-produced torque is

$$dQ = \rho Bc \frac{W^2}{2} C_x dr \tag{4-9}$$

Combining these relations

$$\frac{a'}{1+a'} = \frac{BcC_x}{4\pi r \sin 2\phi} \tag{4-10}$$

If suitable airfoil sectional performance data is available, then the local flow conditions at a given radial station r may be determined by the following procedure:

Given r, c , $C_L(\alpha)$,. $C_D(\alpha)$, θ, V_∞, Ω

A. Guess a and a′ (a = a′ = 0 is acceptable to start)

B. Calculate ϕ (4-2)

C. Calculate α (4-1)

D. Calculate C_L and C_D

E. Calculate C_x and C_y (4-3 and 4-4)

F. Calculate a (4-7)

G. Calculate a′ (4-10)

H. Go back to step B and repeat

Once the above iteration converges the sectional flow properties are known and the local contributions to torque and axial force may be integrated to determine the overall torque and axial force of the rotor. Blade airfoil section changes, twist and blade taper may be accommodated quite readily.

The expressions developed so far required some modifications and qualification. First, to qualify the above procedure, note the flow patterns illustrated below in Figure 4-6. It may be seen that recirculating flow may occur. Such a flow pattern is not consistent with the assumptions leading to equations (4-7) and (4-10), therefore, the above analysis is not valid. A

criterion for determining the onset of recirculating flow may be obtained from wake momentum considerations. The velocity in the wake $u_1 = V_\infty(1 - 2a)$, hence for $a > \frac{1}{2}$, recirculation can occur. This consideration will be modified in the next section. A helicopter, in going from vertical ascent to autorotational descent can pass through the various states illustrated in Figure 4-6. Glauert (10) used experimental results to quantify the turbulent windmill and vortex ring states of a rotor.

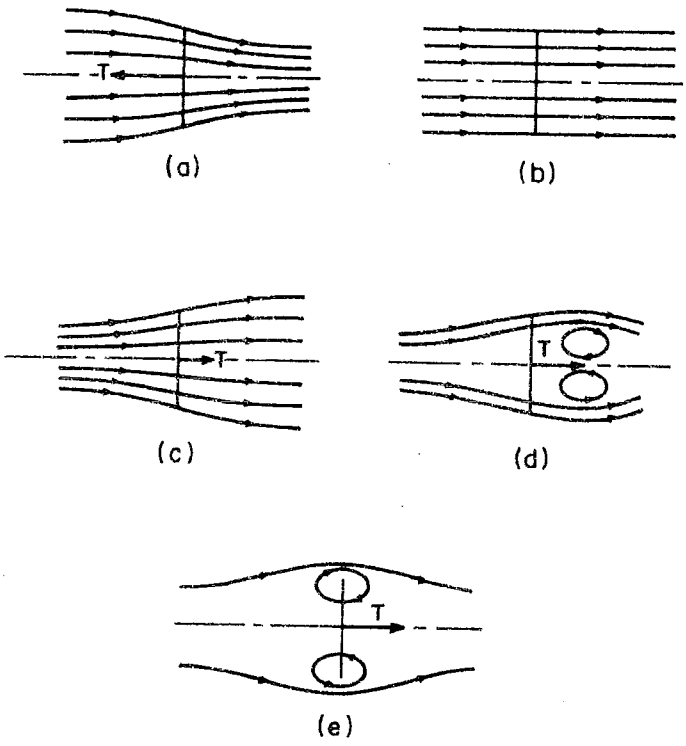

Figure 4.6 Working States of a Rotor: (a) propeller; (b) zero-thrust; (c) windmill; (d) turbulent windmill; (e) vortex ring

4.3 TIP LOSS MODELS

The previous analysis requires some modification because of the pattern of shed vorticity. The flow at any radial position has been assumed to be two dimensional. Radial acceleration and wake-induced flow at the tip can alter the assumed flow pattern. The effects of radial acceleration can be neglected for most wind power machines; however, the wake effects cannot be neglected. So-called tip losses have been treated in a variety of approaches, the simplest of these being to reduce the maximum rotor radius to some fraction of the actual radius, characteristically on the order of 97% of the actual radius. Prandtl (11) and Goldstein (12) have analyzed flow about lightly-loaded propellers (negligible wake contraction) and developed models for the reduction of circulation due to wake interaction at the tips. The result of Prandtl's and Goldstein's approach is circulation-reduction factor F, such that

$$F \equiv \frac{B\Gamma}{\Gamma_\infty} \tag{4-11}$$

where B is the number of blades, Γ is the circulation at a radial station r and Γ_∞ is the corresponding circulation for a rotor with an infinite number of blades. The factor F is a function of tip speed ratio, number of blades and radial position. Of the two models the Goldstein model is the more accurate however, since Goldstein's flow model involves an infinite series of modified Bessel functions, it is more difficult to use. Since there is little difference in results for situations involving three or more blades, the Prandtl model which yields a simple solution can be used.

The incorporation of the tip loss factor into equation for induced velocities proceeds as follows.

The physical meaning of the tip correction is virtually that the maximum change of axial velocity, (V_∞ - u_1) or $2aV_\infty$, in the slipstream occurs only on the vortex sheets and the average velocity change is only a fraction F of this velocity. Thus the velocity change $2aV_\infty$ becomes $2aFV_\infty$ and in similar manner, the angular velocity change is written $2a'F\Omega$. Equations (4-7) and (4-10) then become

$$\frac{a}{1-a} = \frac{\sigma C_y}{8F \sin^2 \phi} \tag{4-12}$$

$$\frac{a'}{1+a'} = \frac{\sigma C_x}{8F \sin \phi \cos \phi} \tag{4-13}$$

where F is the Goldstein tip correction or the Prandtl tip correction factor and the quantity α is a local solidity given by $\sigma \equiv \frac{Bc}{\pi r}$. A further refinement of the analysis can be made in the axial flow velocity u through the rotor disk in equation (4-5) is assumed to vary in the same manner as the wake velocity. The average flow velocity through the rotor is then given by $u = V_\infty(1 - aF)$. Equation (4-13) remains the same, however, equation (4-12) becomes a quadratic

$$(1-aF)aF = \frac{\sigma C_y}{8\sin^2 \phi} \tag{4-14}$$

The derivation of equations (4-13) and (4-14) is given in Appendix II.

The use of equation (4-14) in lieu of (4-12) yields slightly higher performance and significant reduction in the number of iterations required for convergence. It may be noted that the criteria for recirculating flow becomes $aF > ½$.

The Goldstein tip correction for a heavily loaded rotor may be determined following the method of Lock (13). Lock's approach bases the calculation of F on the local value of ϕ, so that $F = F(\phi, r/R)$. The angle ϕ defines a local speed ratio via the relation $\mu = \cot^{-1}\phi$. The corresponding tip speed ratio is $\mu_\infty = R\mu/r$ and thus the Goldstein tip correction factor $F = F(\mu,\mu_\infty)$ can be determined. As a practical consideration it may be noted that at low tip speed ratios the tip loss is appreciable over the entire blade. In such cases this approach ceases to be a tip loss correction, instead being a dominant factor in the calculations. Prandtl's F factor is given by

$$F = \frac{2}{\pi}\cos^{-1}\left[\exp(-f)\right] \tag{4-15}$$

where

$$f = \frac{B}{2}\frac{R-r}{R\sin\phi} \tag{4-16}$$

As the factor F has been derived for a frictionless rotor with optimum distribution of circulation along the blade, the approximate nature of the previous analysis should be noted.

Figure 4-7 gives the calculated power coefficient of the Smith-Putnam Wind Turbine (1) as a function of tip speed ratio. The Smith-Putnam turbine employed an NACA 4418 airfoil which has discontinuously twisted 5° along a 65 foot length. The turbine diameter was 175 feet with an 11′4″ chord. The Goldstein tip correction was used to develop the curve.

The effect of pitch angle can be seen in Figure 4-7. Increased pitch reduces the maximum power but can increase the power available at low tip speed ratios. Figure 4-7 also can be used to illustrate some generalizations concerning wind machines. At low tip speed

ratios, the power coefficient is strongly influenced by the maximum lift coefficient. The angle ϕ is large at low tip speed ratios and much of the rotor, particularly the inboard stations, can be stalled when operating below the design speed. At tip speed ratios above the peak power coefficient, the effect of drag becomes dominant. A high drag coefficient will result in a rapid decrease in power with increasing angular velocity. Finally at some large tip speed ratio the net power output will become zero. If the slope of the power curve at $C_p = 0$ is negative, the rotor operation at zero power output (feathered) will be stable, since for constant wind velocity, decreased rotational speed will result in positive power output which in turn will return the rotor to its original speed. The steeper the curve, the greater the stability.

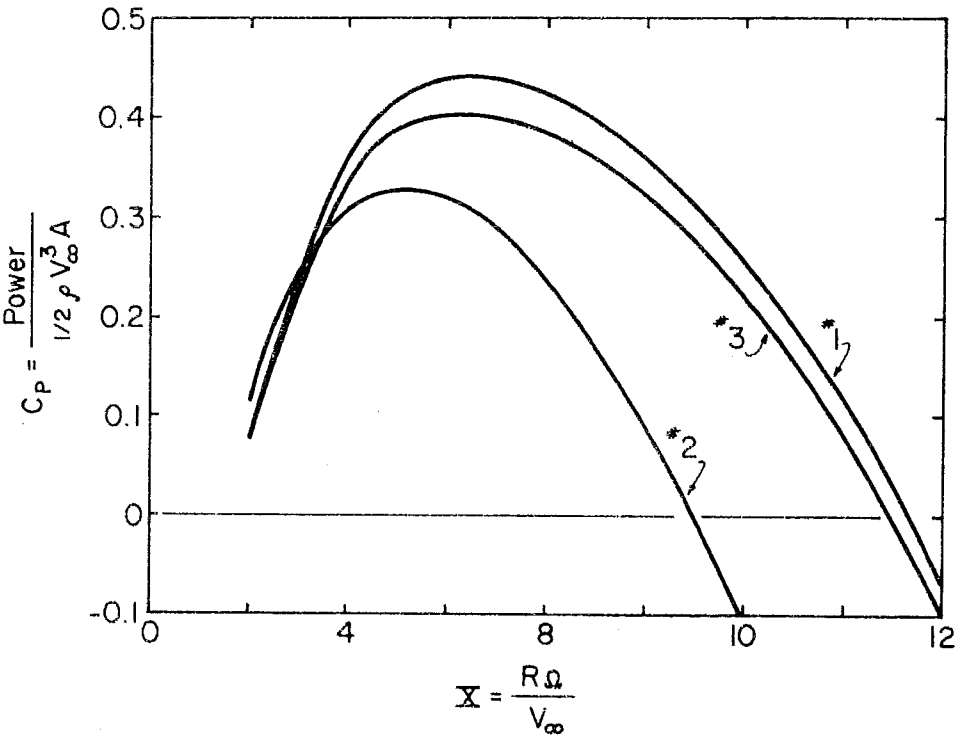

Figure 4.7 Calculated Performance of the Smith-Putnam Wind Turbine.
1) $\theta_{pitch} = 0°$, equations (4-13) and (4-14)
2) $\theta_{pitch} = 5°$, equations (4-12) and (4-13)
3) $\theta_{pitch} = 0°$, equations (4-12) and (4-13)

A plot of power coefficient versus tip speed ratio yields information concerning power output, efficiency, and rotation speed for a given wind velocity. Another type of display that illustrates rotor performance is a plot of power versus wind velocity. Retaining C_p and X as our variables, the power is directly proportional to C_p/X^3 while velocity is given by 1/X. Figure 4.8 illustrates the Smith-Putnam wind turbine calculations shown in Figure 4-7.

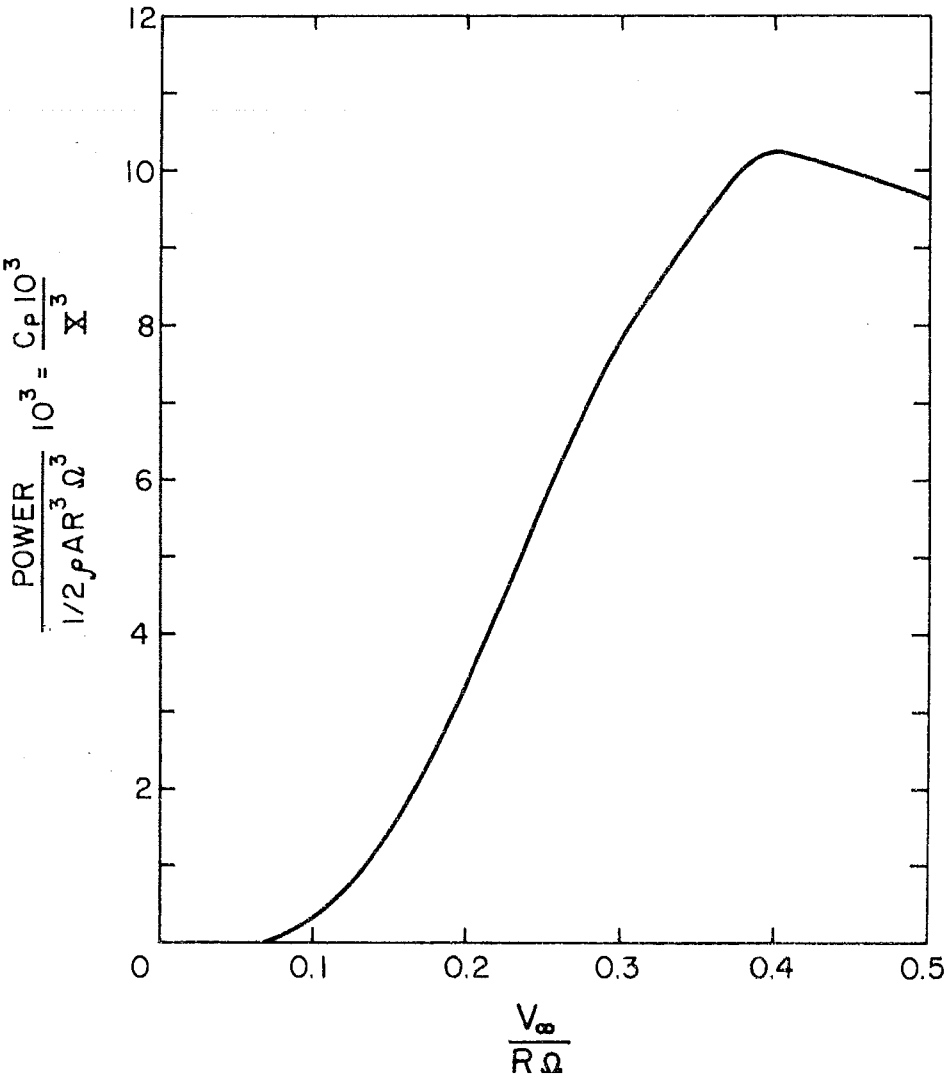

Figure 4.8 Power Output Versus Wind Speed For the Smith-Putnam Wind Turbine $\theta_p = 0°$.

Note that at constant RPM and pitch angle, the stall controls the maximum power output and drag controls the starting velocity. Another point of considerable importance is the location of maximum power coefficient. Operation near the point of maximum power coefficient will give the greatest increase in power for a given increase in wind velocity and hence the greatest sensitivity to wind speed fluctuations.

4.4 THE OPTIMUM ROTOR; GLAUERT

Glauert has developed a simple model for the optimum windmill. The approach used is to treat the rotor as a rotating actuator disk (i.e., corresponds to a rotor with an infinite number of blades) and set up an integral for the power. The power integral is made stationary subject to an energy constraint; the results yielding the maximum power output for a given tip speed ratio.

The relation for the power coefficient is

$$C_p \equiv \frac{P}{\frac{1}{2}\rho V_\infty^3 \pi R^2} = \frac{8}{X^2}\int_0^X (1-a)a'x^3 dx \tag{4-17}$$

where

$$x = \frac{r\Omega}{V_\infty}\ , \quad X = \frac{R\Omega}{V_\infty}\ , \quad a = \frac{V_\infty - u}{V_\infty} \quad \text{and} \quad a' = \frac{\omega}{2\Omega}$$

Since the integral for the power involves two dependent variables, another relation is required. This is the energy equation

$$a'(1-a')x^2 = a(1-a) \tag{4-18}$$

Perhaps the most unique way of illustrating this relation is to consider the velocities at the rotor plane. The flow is assumed to be uniform in annular streamtubes with no circumferential variations. Under these conditions, two-dimensional flow may be assumed.

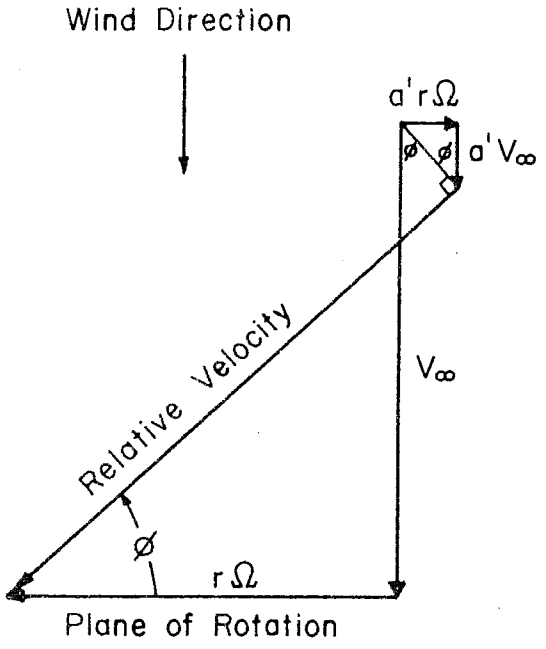

Figure 4.9 Velocity Diagram

In .the absence of drag, the velocity induced at the rotor must be due to lift and hence perpendicular to the relative velocity. Two expressions for tan ϕ may be developed under the condition that the total induced velocity is normal to the relative velocity. These are

$$\tan\phi = \frac{(1-a)V_\infty}{(1+a')r\Omega} = \frac{a'r\Omega}{aV_\infty} \tag{4-19}$$

So that

$$a'(1+a')x^2 = a(1-a) \tag{4-18}$$

The variational problem is now posed

$$C_p = \int_0^X F(a, a', x)dx \tag{4-20}$$

With $G(a, a', x) = 0 = a'(1 + a')x^2 - a(1 - a)$

The solution yields

$$a' = \frac{1-3a}{4a-1} \tag{4-21}$$

so that

$$a'x^2 = (1-a)(4a-1) \tag{4-22}$$

Hence, $1/3 \geq a \geq 1/4$. The variation in a, a', $a'x^2$, and x are given in Table 4.1. Since high speed rotors easily reach tip speed ratios of 7 or more, it can be seen that most of an ideal rotor

Table 4.1 Flow Conditions For The Optimum Actuator Disk

a	a'	$a'x^2$	x
.25	∞	0	0
.27	2.375	.0584	0.157
.29	0.812	.1136	0.374
.31	0.292	.1656	0.753
.33	0.031	.2144	2.630
1/3	0	.2222	∞

will operate with a = 1/3 and the rotational velocity distributed in the form of an irrotational vortex i.e. as $x \to \infty$, $a'x^2 \to (2/9) = \frac{\omega r^2}{2\Omega}\frac{\Omega^2}{V_\infty^2} = \frac{rV_t}{2}\frac{\Omega}{V_\infty^2}$. The power coefficient for various tip speed ratios is given in Table 4.2. At low tip speed ratios the power coefficient is low because of the large rotational kinetic energy in the wake. At large tip speed ratios, the power coefficient approaches 0.593 and the wake rotation approaches zero. The variation of C_p with tip speed ratio is illustrated in Figure 1.6.

Table 4.2 C_p vs X For The Optimum Actuator Disk

$\frac{R\Omega}{V_\infty}$	C_p
0.5	.288
1.0	.416
1.5	.480
2.0	.512
2.5	.532
5.0	.570
7.5	.582
10.0	.593

Further information may be obtained from this model using the blade element theory. As the quantities a and a′ are known for each radial position, the relative velocity and the angle ϕ may be determined. Figure 4.5 may be used to illustrate the velocities and forces in relation to the blade configuration. Of course, since we have assumed that the drag is zero, the only force that acts on the blade is lift.

The incremental thrust and torque acting on an annulus containing B blades each having chord c are given by

$$dT = \frac{Bc}{2} \rho W^2 C_L \cos \phi \, dr \tag{4-23}$$

and

$$dQ = \frac{Bc}{2} r\rho W^2 C_L \sin \phi \, dr \tag{4-24}$$

The momentum expressions yield (assuming b = 2a)

$$dT = 4\pi\rho V_\infty^2 (1-a) a dr \tag{4-25}$$

$$dQ = 4\pi r^3 \rho V_\infty \Omega (a-a) a' dr \tag{4-26}$$

So that

$$\frac{a'}{1-a} = \frac{BcC_L \cos \phi}{8\pi r \sin^2 \phi} \tag{4-27}$$

$$\frac{a'}{1+a'} = \frac{BcC_L \sin \phi}{8\pi r \sin \phi \cos \phi} \tag{4-28}$$

Now a and a′ are known as a function of x so that the shape of the blades may be determined. Table 4.3 gives the results. It may be noted that an optimum blade for a given X and constant C_L will have a chord that approaches a maximum at $x \cong .7$.

Table 4.3 Blade Parameters For The Optimum Actuator Disk

ϕ	x	$\frac{Bc\Omega C_L}{2\pi V_\infty}$
50	0.35	.497
30	1.00	.536
20	1.73	.418
15	2.43	.329
10	3.73	.228
7	5.39	.161
5	7.60	.116

4.5 VORTEX THEORY

The flow over real-rotors differs in many respects from the flow model used to describe the optimum actuator disk. A frequently-used model involves the use of bound vortices to represent lift. Following the concepts of vortex theory as applied to wings, each blade of the rotor is modeled as a bound vortex line. This simple scheme enables the induced flow at each section to be determined via the Biot-Savart Law. However, one may note that the induced flow will vary chordwise over the blade section. In order to fully represent the flow, the blade should be replace by a bound vortex sheet in lieu of a vortex line. Since most windmill rotors have very low solidity, the chordwise variation in flow may be neglected without loss of accuracy.

In this scheme, the bound vorticity serves to produce the local lift on the blade while the trailing vortex filaments induce velocities at each element of the blade. Several solutions for the induced volocity at a blade element have been obtained by solving partial differential equations, but the most straightforward method is a direct integration of the Biot-Savart Law. Now as

straightforward as this method may appear, it requires as an input the knowledge of the trajectory of the vortex filaments in the wake. Since the wake will consist of the superposition of a large array of vortex filaments, each acting on each other, the vortex trajectory (or configuration) cannot be established unless all the vortices are coupled. Now in Prandtl Lifting-Line Theory, the wake is assumed to lie in the plane of the wing and although one can calculate physically impossible velocities which flow thru the vortex sheet wake, the results of Prandtl's theory gives very acceptable answers. Just as the wake from a wing is a vortex sheet (which happens to roll up a snort distance downstream of the wing), the wake shed by a propeller may also be considered as a vortex sheet (which also rolls up in the wake). This approach may be likened to that used in elementary strength of materials where one assumes a deformation geometry and calculates forces – here we assume wake geometry and calculate induced velocities.

For an optimum rotor using vortex theory the Betz criteria (23) may be used. This criteria requires the wake to move back as a rigid screw surface. The writings of Betz, Theodoresen (24), Lerbs (25), and Weinig (26) cover analytical techniques required to define the optimum propeller.

CHAPTER 5

CROSS-WIND AXIS MACHINES

5.1 VORTEX MODELING OF THE WAKE

Continuing the approach discussed in Section 4.1, it is of interest to construct the vortex system of a crosswind axis actuator, since this has not been discussed in the literature.

We note first that if we assume the device to be modeled simply as an oscillating actuator disc of cross section as the device are shed and a wake system similar to that of the rotor actuator disc develops. Again we see that this may be an acceptable model for a many-bladed high tip speed ratio system.

To construct a somewhat more realistic model, consider a crosswind axis machine having slender lifting blades, and for simplicity assume these do not move in a circular path about the axis, but are constrained to follow a square path at constant velocity and at zero angle of attack relative to the path. This model is shown in Figure 5.1. As a blade moves up the leeward sector, it sheds a starting vortex and a trailing pair as shown, and finally sheds its bound vortex as it assumes zero lift over the upper portion of the path. On passage across the forward portion a similar situation occurs. Thus the final wake system appears as shown in Figure 5.2. Note that the crisscross system on the sides will converge to a simple ring type system; that is, the streamwise vorticity component will cancel as the tip speed ratio and blade number is increased.

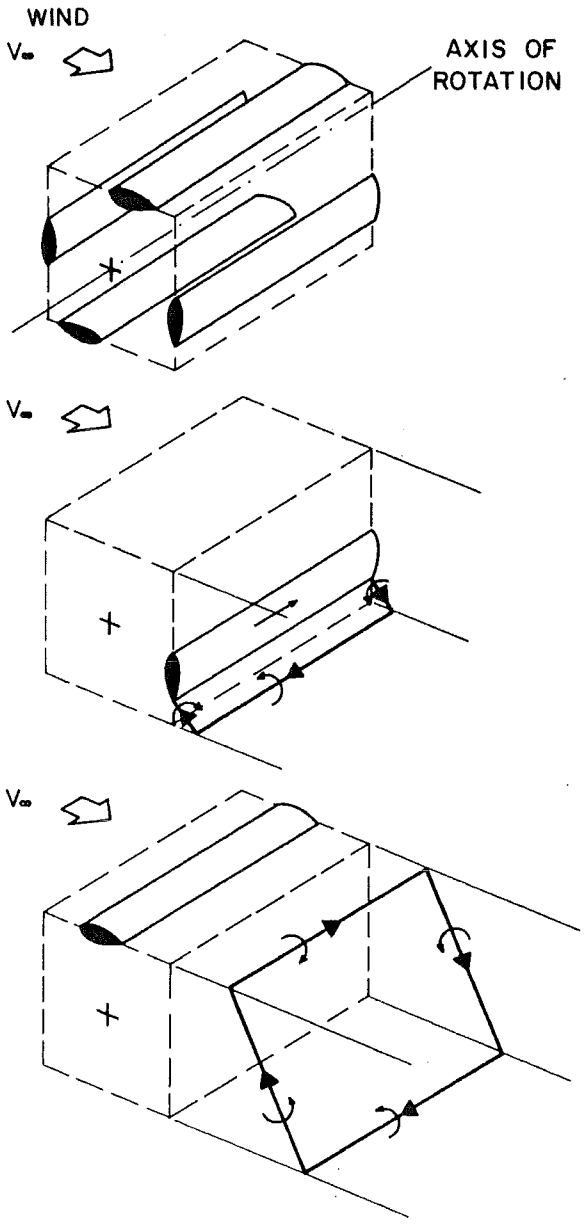

Figure 5.1 Vortex Shedding of Cross-Wind Axis Actuator

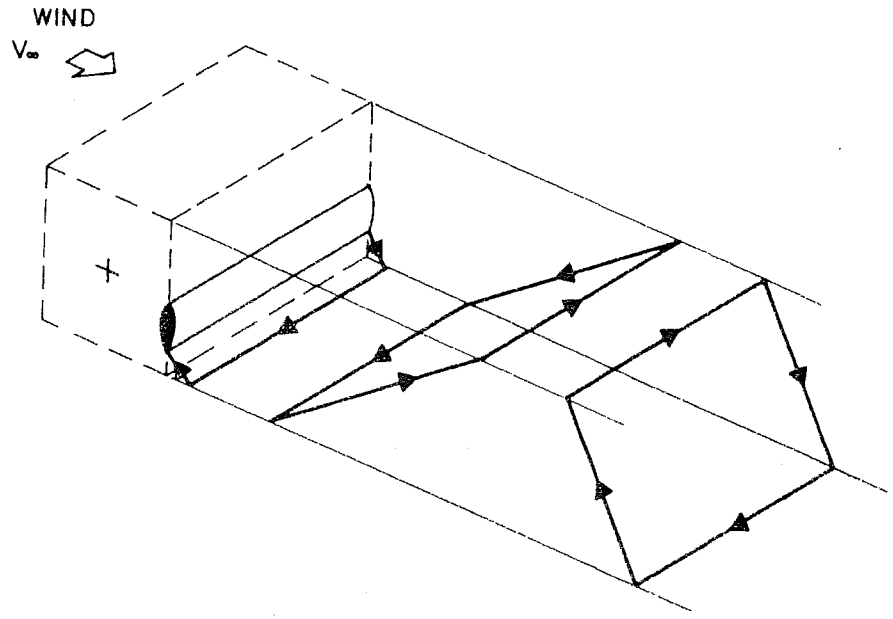

Figure 5.2 Vortex System of Single Bladed Crosswind Axis Actuator

It can be shown that the solution for the induction of an infinite vortex tube of arbitrary cross section is the same as that of one of circular cross section, a uniform internal axial flow, and zero external flow.

If we now consider the more realistic case of a crosswind axis system where the blades rotate about a fixed axis, then the lift and consequently the shed trailing and starting vorticity is continually changing. Adopting arguments similar to those used for the square path system and assuming high advance ratios, we now obtain a wake vortex system as sketched in Figure 5.2. This is importantly different from the previous case since there is internal spanwise vorticity within the tube. It can easily be shown that this spanwise vorticity is linearly distributed across the tube and that the induced internal axial flow is not uniform. Thus it appears that even an ideal cross-axis machine cannot achieve the ideal power coefficient of a wind axis system, since the induced axial flow is not uniform.

5.2 DARRIEUS ROTOR

To analyze a Darrieus-type crosswind-axis device we adopt the standard approach of wing theory, which is to express the forces on the system by a momentum analysis of the wake as well as by an airfoil theory at the lifting surface itself. The expression for these forces contains unknown induced flows. By equating the wake and wing forces one obtains sufficient equations to determine the induced flows.

For the device considered we assume that each spanwise (parallel to the axis) station behaves quasi-independently in the sense that the forces on the device at each station may be equated to the wake forces. In general, these devices can experience a windwise as well as a cross-wind force, so that the wake can be deflected to the side.

Consistent with vortex theory, we will assume the induced flows at the device are one half their value in the wake. Thus we obtain that if the wake windwise perturbation is $2aV_\infty$, then at the device itself the incoming flow has velocity $V_\infty(1 - a)$, giving the flow system illustrated in Figure 5.3.

In order to simplify the analysis we shall adopt the following assumptions,

1. $\beta = 0$
2. $C_D = 0$
3. $C_L = 2\pi \sin \alpha$
4. $c \ll R$

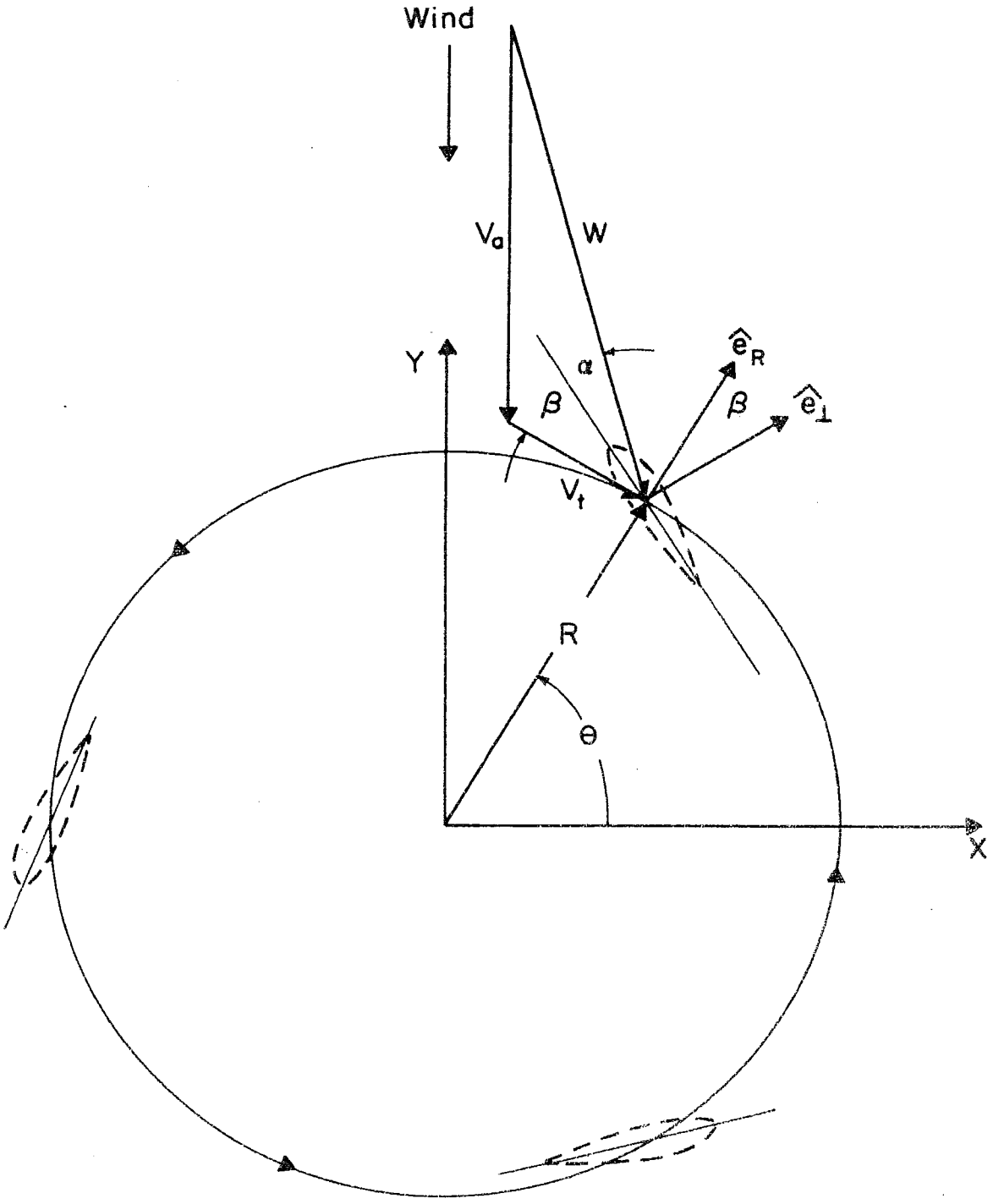

Figure 5.5 Flow System for a Crosswind-Axis Turbine

Our results will then be limited to an inviscid analysis at high tip speed ratios where the maximum angle of attack α is small. The low tip speed ratio performance requires numerical analysis to model the nonlinear aerodynamics near stall. Using the above assumptions and starting with the Kutta-Joukowski law, we can write

$$L = \rho W \Gamma = \tfrac{1}{2} \rho W^2 c C_L \tag{5-1}$$

so that

$$\Gamma = \frac{c}{2} W C_L = \pi c W \sin \alpha \tag{5-2}$$

Since the force on the airfoil can be expressed as

$$\vec{F} = \rho \vec{W} \times \vec{\Gamma} \tag{5-3}$$

we obtain

$$\vec{F} = \rho \pi c \left[- V_a V_t \sin^2 \theta \, \hat{j} - \left(V_a^2 \sin \theta + V_a V_t \sin \theta \cos \theta \right) \hat{i} \right] \tag{5-4}$$

Now we can equate the force on the airfoil to the momentum lost in the streamtube which the airfoil occupies. Let the streamtube be of width dx when the airfoil goes from angular position θ to position $\theta + d\theta$. The width dx is related to $d\theta$ by

$$dx = R d\theta \left| \sin \theta \right| \tag{5-5}$$

The process will repeat itself every revolution so the time interval of our analysis shall be one period which is $2\pi/\Omega$. Of this time period, the airfoil will spend a time increment of $d\theta/\Omega$ in

the front portion of the streamtube and another time increment of $d\theta/\Omega$ in the rear portion of the wake. Since the streamwise force contribution from equation (5-4) is seen to be symmetrical with respect to the angles $\pm\theta$ we may write the blade force equation for the time period $2\pi/\Omega$ as

$$dF_{blade} = 2\rho\pi c V_t V_a \sin^2\theta \frac{d\theta}{\Omega} \tag{5-6}$$

Now the momentum equation yields the force in the streamtube as

$$dF_{momentum} = \rho R d\theta \left|\sin\theta\right| (1-a) V_\infty 2 V_\infty a \frac{2\pi}{\Omega} \tag{5-7}$$

Equating these two forces under the assumption that $V_a = V_\infty(1 - a)$ and $V_t = R\Omega$ yields an expression for the axial interference factor a for one blade

$$a = \frac{c}{2R} \frac{R\Omega}{V_\infty} \left|\sin\theta\right| \tag{5-8}$$

or for B blades

$$a = \frac{Bc}{2R} \frac{R\Omega}{V_\infty} \left|\sin\theta\right| \tag{5-9}$$

Now that a is defined, the blade force may be resolved into torque and radial components. The torque is given by

$$Q = \rho\pi c R\, V_\infty^2 (1-a)^2 \sin^2\theta \tag{5-10}$$

The average torque for a rotor with B blades is

$$\overline{Q} = \left[\rho\pi BcRV_\infty^2\right]\left[\tfrac{1}{2} - \frac{4}{3\pi}\frac{BcX}{R} + \frac{3}{32}\left(\frac{BcX}{R}\right)^2\right] \tag{5-11}$$

and the corresponding sectional power coefficient is given by

$$C_p = \pi X \frac{Bc}{R}\left[\tfrac{1}{2} - \frac{4}{3\pi}\frac{BcX}{R} + \frac{3}{32}\frac{B^2c^2X^2}{R^2}\right] \tag{5-12}$$

This expression yields a maximum power coefficient of 0.554 when the quantity $BcX/2R = a_{max} = 0.401$. Further refinements can be made with consideration of drag and maximum angle of attack. The maximum angle of attack occurs approximately at the point $\theta = \pi/2$ where

$$\tan\alpha = \frac{1 - a_M}{X} = \frac{1}{X} - \frac{Bc}{2R} \tag{5-13}$$

When α is set equal to α_{max} we may rearrange equation (5-13) to express the starting tip speed ratio. Using $\alpha_{max} = 14°$ max we obtain

$$X_{start} \doteq \frac{4}{1 + 2\frac{Bc}{R}} \tag{5-14}$$

so that a three-bladed rotor with a one foot chord and a 20 foot radius would have a starting tip speed ratio of about 3.

Since this type of rotor will not operate at low tip speeds, the drag losses may be simple approximated by assuming that the local velocity is $W \cong R\Omega$. The drag torque is then

$$\overline{Q}_D = -\frac{C_D}{2}\rho R^2\Omega^2 BcR = -\frac{C_D}{2}\rho V_\infty^3 \frac{BcX^3}{\Omega} \tag{5-14}$$

and the contribution to the power coefficient is

$$\Delta C_p = -C_D \frac{Bc}{2R} X^3 \tag{5-15}$$

At this point, a solidity may be defined as $\sigma = Bc/2R$, the ratio of blade circumference to disc diameter. The power coefficient becomes

$$C_p = \pi\sigma X - \frac{16}{3}\sigma^2 X^2 + \sigma^3 X^3 \left(\frac{3\pi}{4} - \frac{C_D}{\sigma^2}\right) \tag{5-16}$$

and it may be seen that $C_p = C_p\left(\sigma X, \frac{C_D}{\sigma^2}\right)$.

5.3 THE CIRCULAR ROTOR

At the high rotational speeds required for the Darrieus-type rotor, the inertial loads are large and result in substantial bending loads in the blades. These bending loads may be removed by deploying the blade in a shape similar to the caternary so that the loads are entirely tensile. The required shape has been investigated by Blackwell (22) and given the name troposkien. The curve is described by elliptic integrals and is approximated by a sine curve or parabola. The effect on performance caused by bringing the blades closer to the axis of rotation is substantial since both the rotational speed and the usable component of the lift are reduced. Figure 5.4 below illustrates the troposkien curve and the local angle γ between the blade tangent and the axis of rotation.

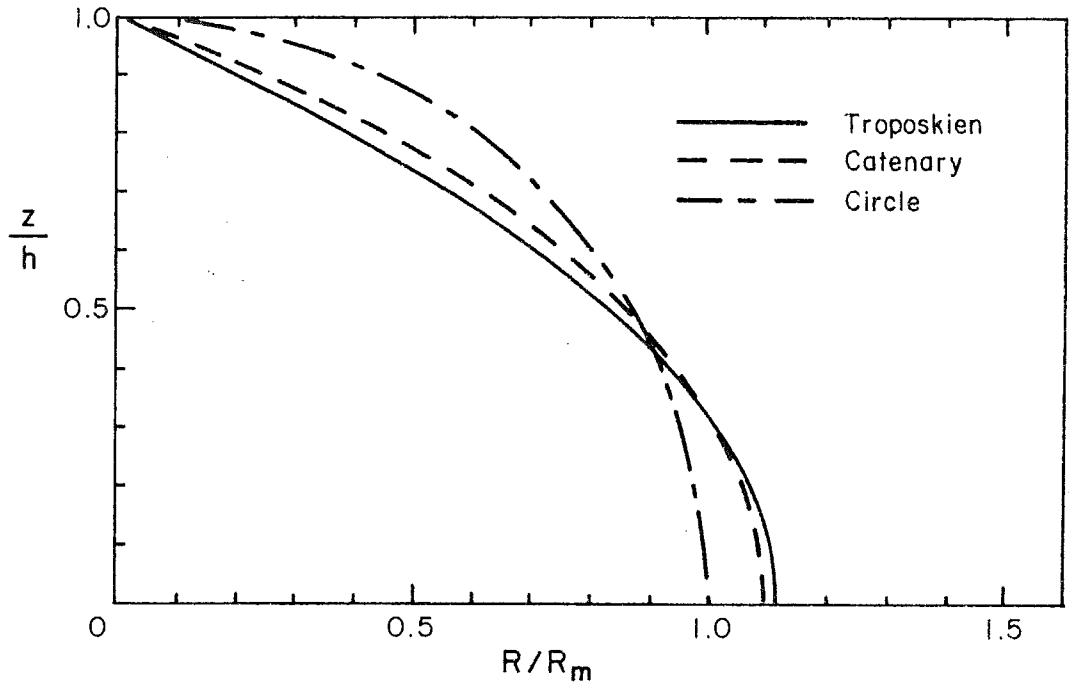

Figure 5.4 Troposkien, Circle and Caternary of Equal Length

The analysis of the curved rotor proceeds in the same manner as in Section 5.2. If we analyze a unit height of the rotor, the expression for a becomes

$$a = \sigma X \cos\gamma \left| \sin\theta \right| \tag{5-17}$$

where the product σX may be taken as the solidity and tip speed ratio at the point $R = R_{max}$ since this product is independent of R. The torque generated by a slice dz along the rotor axis is

$$\frac{d\overline{Q}}{dz} = \rho\pi B c V_\infty^2 \cos\gamma \left[\tfrac{1}{2} - \frac{8}{32}\sigma X \cos\gamma + \frac{3}{8}\sigma^2 X^2 cs^2\ \gamma \right] \tag{5-18}$$

and the incremental power coefficient is

$$\frac{dC_p}{dz} = \frac{d\overline{Q}}{dz}\frac{\Omega}{\frac{1}{2}\rho V_\infty^2 A} = \frac{4\pi\sigma X}{A} R\cos\gamma\left[\frac{1}{2} - \frac{8}{3\pi}\sigma X\cos\gamma + \frac{3}{8}\sigma^2 X^2\cos^2\gamma\right] \qquad (5\text{-}19)$$

The integration of equation (5-19) for an arbitrary geometry may be accomplished; one simple case is the circular blade for which a maximum power coefficient of 0.536 occurs at $\sigma X = a_{max} = 0.461$. The effects of drag and stall can be included in the above model by development of a blade element theory similar to that developed for the wind-axis rotor.

CHAPTER 6

FORCES AND MOMENTS DUE TO VERTICAL WIND GRADIENT

6.1 INTRODUCTION

In the analysis of rotors covered previously, the relative wind was assumed to be uniform and parallel and to be perpendicular to the plane of rotation of the rotor. In reality, both flow irregularities and rotor motion can occur. Real flows will be neither uniform, steady nor unidirectional. Vertical wind gradient, gustiness and-wind turning with elevation all present double-edged difficulties to the design and operation of wind turbines. First, the local flow conditions must be known; secondly, techniques to predict the magnitude of the effects of the flow variations must be adapted to wind machines. The lack of knowledge of local flow conditions, particularly in regions of rough terrain represents a considerable barrier. While some wind gradient data exists for flow over rough terrain, there is little or no data on turbulence spectra and wind turning. Slade (13) has reported the presence of considerable wind turning in the atmospheric surface layer over rough terrain. By contrast the knowledge of flow over flat terrain is much more complete.

Extensive studies have been made of wind structure in the atmospheric surface layer over flat terrain. Monin and Obukhov (14) have developed a relation for the mean flow that encompasses stable, neutral and unstable stratification. Their relation involved three parameters, the surface friction velocity, the surface roughness and a stability parameter, the Monin-Obukhov length. By contrast, the mean flow over rough terrain is frequently approximated by a power law relation with height

$$\frac{V_\infty}{V_R} = \left(\frac{Z}{h}\right)^\eta \tag{6-1}$$

where the coefficient η is less than one. Because of the simplicity of equation (6-1), since it requires fewer parameters, and the fact that the wind variation over a limited range (~ 100 to 200 feet) is required for wind turbines we shall use the above relation.

The departures from the flow studied previously have no first order effects on the turbine mean output, however, periodic variations in torque, time dependent side forces and pitching moments can occur. These forces and moments will effect the overall system dynamics and hence both the design and operation of a wind turbine. In addition to the aerodynamic forces and moments certain mechanical forces and moments are present. This section will deal only with the aerodynamic loads due to wind gradient.

Both rotor yaw and flapping can induce large forces and moments. Rotor yaw can be treated using the analysis of Ribner (15), flapping moments and forces are included in the program described in Appendix I.

6.2 THE EFFECTS OF VERTICAL WIND GRADIENT

A vertical wind gradient will induce forces and moments as illustrated in Figure 6-1. The largest of these are the torque variation and the pitching moment. As would be expected the magnitude of these moments is dependent upon scale, since it is the velocity difference between the top and bottom of the rotor that is significant. Before proceeding further, it should be noted the incremental forces on a blade element have been designated normal (n) and tangential (t) in order to avoid confusion with the coordinates XYZ. Thus the (x,y) of Chapter 4 are now the (t,n) coordinates.

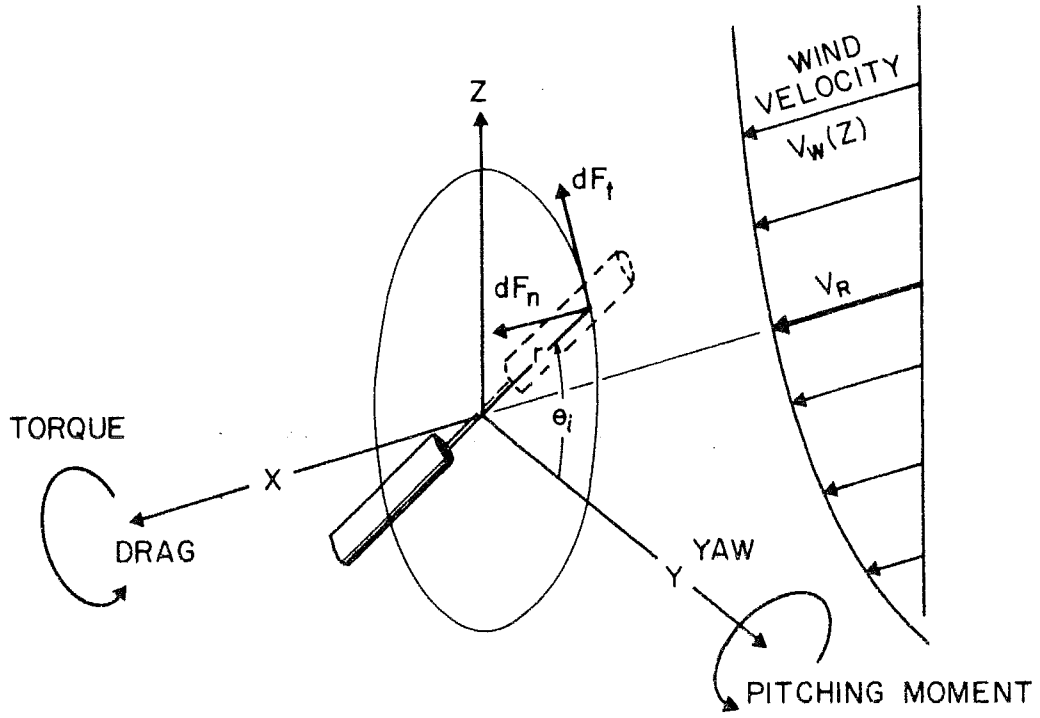

Figure 6.1 Rotor in a Wind Gradient.

Figure 6.2 on the following page illustrates the blade velocity diagram. This velocity diagram differs from previous illustrations in that the freestream velocity V_∞ has been replaced with the local wind velocity V_w.

For a blade in the upper half of the rotor disk, the axial velocity will be higher than for a blade in the lower half disk. The increase in V_w increases both the resultant velocity w and the angle of attack α. At high tip speed ratios it may be seen that the principle effect of increased velocity (due to gradient or gust) will be an increased angle of attack. The variation in angle of attack in turn will cause variations in the force dF_t and dF_n with the angle of rotation. Expressions for the first and second order forces and moments can be generated from the steady-

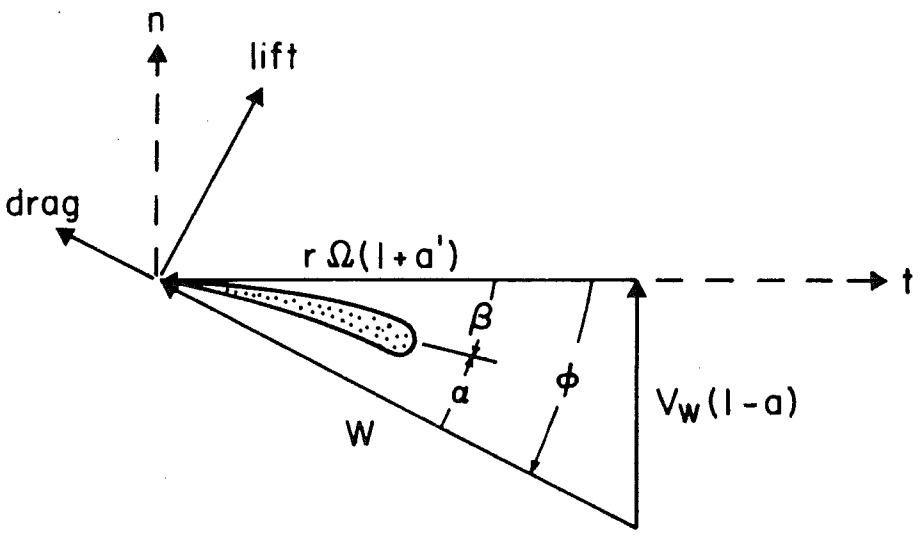

Figure 6.2 Blade Velocity Diagram

state performance aerodynamics in the following manner. The differential force on a rotor element may be expressed in terms of a Taylor Series about the rotor hub so that

$$dF_t\big|_z = dF_t\big|_0 + dF_{t_u} u_z\big|_0 \Delta Z + \left[dF_{t_{uu}} u_z^2 + dF_{t_u} u_{zz}\right]\frac{\Delta Z^2}{2} \cdots \qquad (6\text{-}2)$$

where $dF_{t_u} \equiv \frac{\partial F_t}{\partial u}$, $dF_{t_{uu}} \equiv \frac{\partial^2 F_t}{\partial u^2}$ and $u \equiv \frac{V_w}{V_{ref}}$

A similar expression may be obtained for dF_n. These forces change from their hub values (Z = 0) due to the variation in wind velocity with elevation. The distance $\Delta Z = r\sin\theta_i$, where θ_i refers to the angle of rotation of the ith blade. Rewriting equation (6-2) in the form

$$dF_t = T_0 + T_1 \Delta Z + T_2 \frac{\Delta Z^2}{2} \cdots \qquad (6\text{-}3)$$

and expressing dF_n in the same manner

$$dF_n = N_0 + N_1 \Delta Z + N_2 \frac{\Delta Z^2}{2} \quad \cdots \tag{6-4}$$

we obtain the following forces and moments by integrating over the blade and summing over B blades, where $B \geq 2$.

TORQUE

$$Q = \int r T_0 dr + \int r^2 T_1 dr \sum_{i=1}^{B} \sin\theta_i + \int r^3 T_2 dr \sum_{i=1}^{B} \sin^2 \theta_i \tag{6-5}$$

$\sum_{i=1}^{B} \sin\theta_i = 0$

PITCHING MOMENT

$$M_y = \int r N_0 dr \sum_{i=1}^{B} \sin\theta_i + \int r^2 N_1 dr \sum_{i=1}^{B} \sin^2 \theta_i + \int \frac{r^3 N_2}{2} dr \sum_{i=1}^{B} \sin^3 \theta_i \tag{6 -6}$$

$\sum_{i=1}^{B} \sin\theta_i = 0$

$\sum_{i=1}^{B} \sin^3 \theta_i = 0$ unless B is odd

The summation over B equally spaced blades has been evaluated and it may be noted that wind gradient induces no first or second order yawing moment.

Table 6.1 on the next page gives the values of the summations for various numbers of blades.

The terms N_1, N_2, T_1 and T_2 remain to be evaluated in order to determine the magnitude of the forces and moments. As the method of differentiation is straightforward, let us indicate the approach by evaluation of N_1.

Table 6.1 Trigonometric Sums

	B = 2	B = 3	B = 4
$\sum_{i=1}^{B} \sin^2 \theta_i$	$1 - \cos 2\Omega t$	3/2	2
$\sum_{i=1}^{B} \sin^2 \theta_i \cos \theta_i$	0	$-\frac{3}{4}\cos 3\Omega t$	0
$\sum_{i=1}^{B} \sin^3 \theta_i$	0	$-\frac{3}{4}\sin 3\Omega t$	0

$$N_1 = \frac{\partial(dF_n)}{\partial u}\frac{\partial u}{\partial Z}\bigg|_{Z=0} \Delta Z = \tfrac{1}{2}\rho V_R^2 c\left[\frac{\partial}{\partial u}\left\{\left(u^2+v^2\right)\left(C_L\cos\phi + C_D\sin\phi\right\}\frac{\partial u}{\partial Z}\right]\right|_{Z=0} \Delta Z \quad (6\text{-}7)$$

where $v \equiv r\Omega/V_r$ and $u \equiv \frac{V_W(Z)}{V_R}$. The- differentiation of C_L requires some comment. As $\phi = \beta + \alpha$ and β remains constant

$$\frac{\partial C_L}{\partial u} = \frac{\partial C_L}{\partial \alpha}\frac{\partial \alpha}{\partial \phi}\frac{\partial \phi}{\partial u} = C_{L_\alpha}\frac{\partial \phi}{\partial u} \quad (6\text{-}8)$$

The final result is

$$N_1 = \tfrac{1}{2}\rho V_R^2 c v\left[C_{L_\alpha}\cos\phi + C_L\sin\phi + \frac{C_D\left(1+\sin^2\phi\right)}{\cos\phi}\right]\bigg|_{Z=0}\frac{\partial u}{\partial Z}\bigg|_0 \Delta Z \quad (6\text{-}9)$$

The variation in torque coefficient may be evaluated from the preceding analysis

$$\frac{\Delta Q}{\frac{1}{2}\rho V_R^2 \pi R^3} \equiv \Delta C_Q = \left\{ I_1 \left(\frac{R}{V_R} \frac{dV_W}{dZ}\bigg|_{Z=0} \right)^2 + I_2 \left(\frac{R^2}{V_R} \frac{d^2 V_W}{dZ^2}\bigg|_{Z=0} \right) \right\} \sum_{i=1}^{B} \sin^2 \theta_i \qquad (6\text{-}10)$$

where the integrals I_1 and I_2 are evaluated as

$$I_1 = \frac{1}{\pi} \int_{R_{hub}}^{R} \left[\left(2 - \cos^2 \phi\right) C_L \sin\phi + 2\cos\phi C_{L_\alpha} - 2\cos^3 \phi C_D \right] (1-a)^2 \left(\frac{r}{R}\right)^3 \frac{c}{R} d\left(\frac{r}{R}\right) \qquad (6\text{-}11)$$

and

$$I_2 = \frac{X}{\pi} \int_{R_{hub}}^{R} \left[\left(1 + \sin^2 \phi\right) C_L + C_{L_\alpha} \sin\phi - C_D \sin\phi \right] (1+a')(1-a) \left(\frac{r}{R}\right)^4 \frac{c}{R} d\left(\frac{r}{R}\right) \qquad (6\text{-}12)$$

Similar type integrals are obtained by the other forces and moments. As can be seen from equations (6-11) and (6-12), considerable simplification can be made if the angle ϕ is small and the value of C_L and c are constant over the outer portions of the blades. In this case, closed form approximations can be obtained.

6.3 APPROXIMATE RELATIONS

At high tip speed ratios $\sin\phi \cong \phi$ and by neglecting drag it may be shown that the following expressions may be obtained.

PITCHING MOMENT

$$\frac{M_y}{\frac{1}{2}\rho V_R^2 \pi R^2} = \frac{\sigma X C_{L_\alpha}}{4}(1-a)\frac{R dV_W}{V_R dZ}\bigg|_{Z=0} \sum_{i=1}^{B} \frac{\sin^2\theta_i}{B} \tag{6-13}$$

TORQUE CHANGE

$$\frac{\Delta Q}{\frac{1}{2}\rho V_R^2 \pi R^3} = \left\{ I_1 \left(\frac{R dV_W}{V_R dZ} \right)^2 \bigg|_{Z=0} + I_2 \left(\frac{R^2 d^2 V_W}{V_R dZ^2}\bigg|_{Z=0} \right) \right\} \sum_{i=1}^{B} \frac{\sin^2\theta_i}{B} \tag{6-14}$$

where

$$I_1 \cong \frac{\sigma C_{L_\alpha}(1-a)^2}{2B}$$

and

$$I_2 \cong \left\{ \frac{\sigma X C_L}{5B} + \frac{(1-a)\sigma C_{L_\alpha}}{4B} \right\} (1-a)$$

Some representative values may be obtained by using the data from the Smith-Putnam wind turbine. The long term wind data yield

$$\frac{1}{V_R}\frac{dV_W}{dZ}\bigg|_{Z=0} = \frac{0.104}{h_h} \quad , \quad \frac{1}{V_R}\frac{d^2V_W}{dZ^2}\bigg|_{Z=0} = -\frac{0.14}{h_h^2} \quad , \quad h_h = 120'$$

and using the values listed below

$\sigma = 0.083$ $\quad$ $R = 87.5$ ft.

$X = 6$ $\quad$ $B = 2$

$C_{L_\alpha} = 5.5$ $\quad$ $C_L = 0.6$

$a = 0.33$

we obtain, neglecting the flapping motion of the Smith-Putnam machine,

PITCHING MOMENT

$$\frac{M_y}{\frac{1}{2}\rho V_R^2 \pi R^3} = 0.0173\left(1 - \cos 2\Omega t\right) \tag{6-15}$$

TORQUE VARIATION

$$\frac{\Delta Q}{\frac{1}{2}\rho V_R^2 \pi R^3} = -0.00153\left(1 - \cos 2\Omega t\right) \tag{6-16}$$

The numbers are difficult to judge. Accordingly, let us reference the forces to the drag of the wind turbine and the moments to the torque.

$$D = C_T \tfrac{1}{2}\rho V_R^2 \pi R^2 \quad , \quad C_T \cong \frac{2}{3}$$

$$Q = C_Q \tfrac{1}{2}\rho V_R^2 \pi R^3 \quad , \quad C_Q = \frac{C_p}{X} \quad , \quad C_p = 0.4$$

PITCHING MOMENT

$$\frac{P}{Q} = 0.259\left(1 - \cos 2\Omega t\right) \tag{6-17}$$

TORQUE VARIATION

$$\frac{\Delta Q}{Q} = -0.023\left(1 - \cos 2\Omega t\right) \tag{6-18}$$

The yaw and drag forces are quite insignificant while the pitching moment is seen to be quite appreciable, amounting to a variation of 52% of the value of the torque. The torque variation is seen to be up to a 4.6% decrease in torque and hence also power. The torque variation itself requires more discussion. Equation (6-14) gives an expression for the torque change which may be modified to express the percentage torque change.

Adopting the power 1 aw profile given by equation (6-1) we obtain

$$\frac{\Delta C_Q}{C_Q} = -\frac{X\sigma(1-a)^2 C_{L_\alpha}}{4C_p}\left(\frac{R}{h}\right)^2 \left\{-2\eta^2 + \left\{\frac{4XC_L}{5(1-a)C_{L_\alpha}} + 1\right\}\eta(1-\eta)\right\} \sum_{i=1}^{B} \frac{\sin^2\theta_i}{B} \tag{6-19}$$

where h is the height of the rotor hub. The effects of scale, tip speed ratio, solidity and load maybe estimated from equation (6-19). For example a rotor operating at constant RPM at wind speeds below the design point will have large X and low C_p. The torque variation for large scale will be appreciable.

It may be noted that the bracketed expression in equation (6-19) is approximately equal to $\eta - 3\eta^3$. This expression has a maximum value when $\eta = 1/6$. Experimental evidence for flow over smooth terrain yields $\eta \cong 0.17$.

The expressions developed for the torque variation may also be used to evaluate the change in power output due to wind gradient. The variation in torque due to the wind gradient is approximately constant over a wide range of tip speed ratios. The net output of a wind turbine however changes appreciably with tip speed so that the percentage variation in turbine output due to wind gradient (or gust) increases greatly as the net turbine output approaches zero. Figure 6.3 on the following page illustrates the percentage decrease in mean turbine output due to wind gradient for the Smith-Putnam wind turbine. Flapping motion of the blades was not included in this example. The absolute magnitude of the power variation due to gradient may be obtained by using the results of Figure 6.3 along with Figure 4.8.

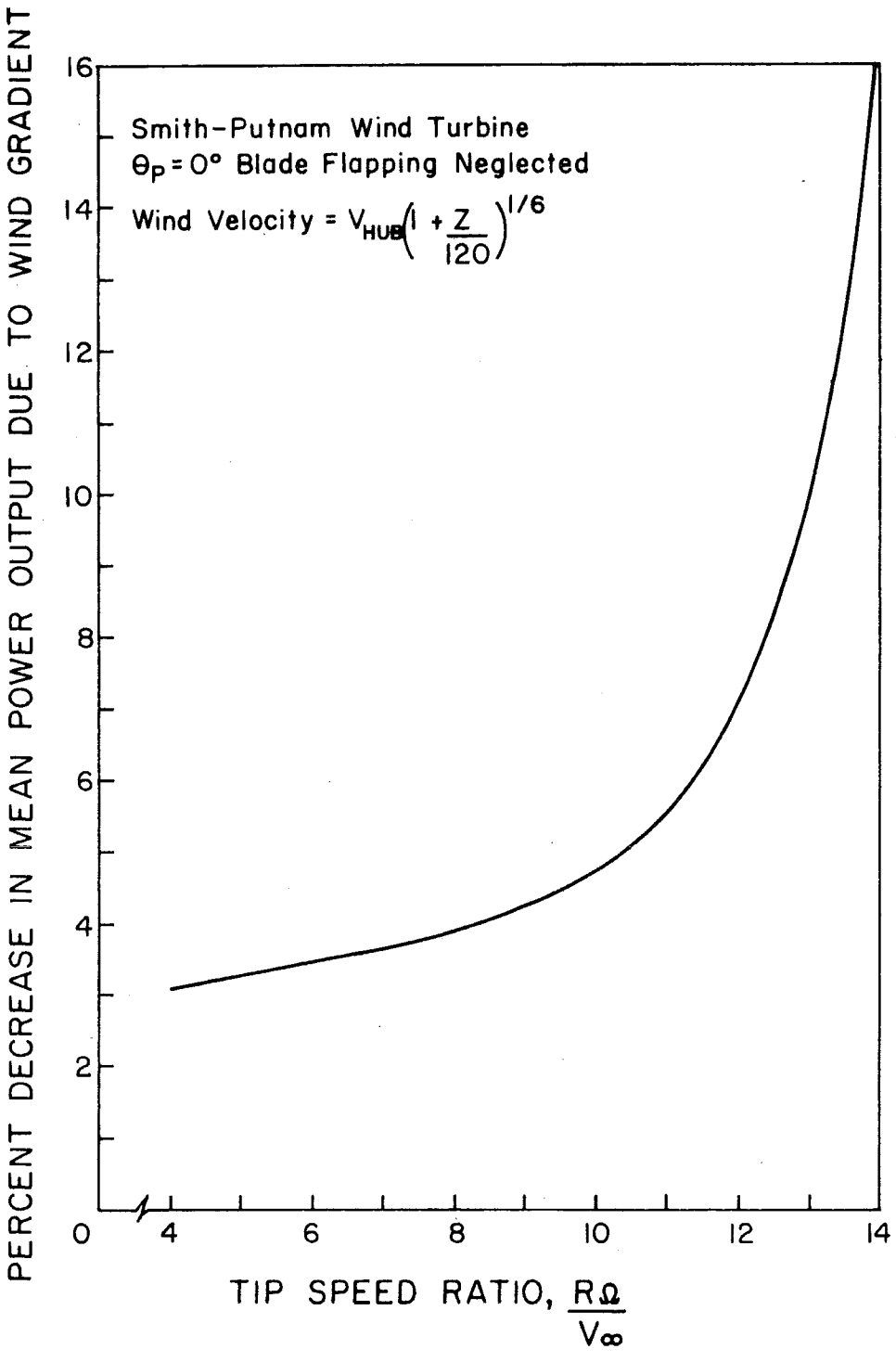

Figure 6.3 Percent Reduction In Power Output Due To Wind Gradient

References

1. Putnam, P. C. Power From the Wind, VanNostrand Company, Inc. New York, 1948.

2. N.Y.U., Final Report on the Wind Turbine. Office of Production, Research and Development, War Production Board, PB25370, Washington, D.C., January 31, 1946.

3. Golding, E. W., The Generation of Electricity by Wind Power, Philosophical Library, New York, 1956.

4. Rankine, W. J., Transactions, Institute of-Naval Architects, Vol. 6, p. 13, 1865.

5. Froude, W., Transactions, Institute of Naval Architects, Vol. 19, p. 47, 1878.

6. Froude, R.E., Transactions, Institute of Naval Architects, Vol. 30, p. 390 ,1889.

7. Joukowski, N. E., Travanx du Bureau des Calculs et Essais Aeronatuiques de l'Ecole Superieure Technique de Moscou, 1918.

8 Goorjian, P. M., AIAA Journal, Vol. 10, No.4, April, 1972, p. 543-4.

9 Glauert, H., Aerodynamic Theory (W. F. Durand, Editor-in-chief), Vol. 6, Division L, p. 324. Julius Springer, Berlin 1935.

10. Glauert, H., The Analysis of Experimental Results in the Windmill Brake and Vortex Ring States of an Airscrew, Br. R & M 1026, 1926.

11. Prandtl, L., Appendix to Schraubenpropellor mit gerngstein Energieverlust, by A. Betz, Gottinger Nachr. p. 193-217, 1919.

12. Goldstein, S., On the Vortex Theory of Screw Propellors, Roy. Soc. Proc. (A) 123, p. 440, 1929.

13. Slade, D. H., Journal of Applied Meteorology, Vol. 8, April 1969, p. 293-7

14. Monin, A. S. and Obukhov, A. M., Basic Laws of Turbulent Mixing In the Ground Layer of the Atmosphere, translated from Akademiia Nauk SSSR, Leningrad, Geofizicheskii Institut, Trudy, Vol. 151, No. 24, 1954, pp 163-187.

15. Ribner, N. S., Propellers in Yaw, NACA Report 820, Washington, D.C., 1948.

16. Shapiro, J., Principles of Helicopter Engineering, McGraw-Hill, New York, 1955.

17. Wolkovitch, J., Analytical Prediction of Vortex Ring Boundaries for Helicopters in Steep Descents. J. Amer. Helicopter Soc., Vol. 17, No.3, 1972.

18. Lock, C. N. H., H. Bateman, and H. C. H. Townend, An Extension of the Vortex Theory of Airscrews with Applications in Airscrews of Small Pitch, Including Experimental Results. Br. A.R.C., R. & M 1014. 1925.

19. Lilley, G. M. and W. J. Rainbird, A Preliminary Report on the Design and Performance of Ducted Windmills. Cranfield, CoA Report No. 102, 1956.

20. South, P. and Rangi, R., The Performance and Economics of the Vertical-Axis Wind Turbine Developed at the National Research Council, Ottawa, Canada, Presented at the 1973 Annual Meeting of the Pacific Northwest Region of the American Society of Agricultural Engineers, Calgary, Alberta, October 10-12, 1973.

21. Kuchemann, D., and J. Weber, Aerodynamics of Propulsion, McGraw-Hill, New York, 1953.

22. Blackwell, B. F., and Reis, G. E., Blade Shape for a Troposkien Type of Vertical-Axis Wind Turbine, Sandia Laboratories Energy Report SLA-74-0154, April, 1974, Albuquerque, New Mexico.

23. Bet z, A., 1919, "Schraubenpropeller mit Geringstem Energieverlust," Nach. der Kgl. Gesellschaft der Wiss. zu Gottingen, Math.-Phys. Klasse, pp. 193-217; reprinted in Vier Abhandlungen zur Hydrodynamik und Aerodynamik by L. Prandtl and A. Betz, Gottingen, 1927 (reprint Ann Arbor: Edwards Bros., 1943), pp. 68-92.

24. Theodorsen, Theodore, Theory of Propellers, McGraw-Hill Book Co.; Inc., New York, 1948.

25. Lerbs, H. W., 1952, "Moderately Loaded Propellers with a Finite Number of Blades and an Arbitrary Distribution of Circulation," Trans. Soc. Naval Architects and Marine Engrs., 60, 73-117.

26. Weinig, F., 1935, Die Stromung um die Schaufeln von Turbomaschinen. Leipzig: J.A. Barth.
_____, 1939/1948, Aerodynamics of the Propeller, trans. from 1939 German book, Aerodynamik der Luftschraube and revised by Author. Dayton, Ohio: Air Documents Div. Air Atl. Command.

Symbols

A	Projected rotor disc area
a	Axial interference factor at the rotor $a \equiv 1 - u/V_\infty$
a′	Tangential interference factor at the rotor $a' \equiv \omega/2\Omega$
B	Number of blades
b	Axial interference factor in the wake $b \equiv 1-u_1/V_\infty$
c	Blade chord
C_L	Sectional lift coefficient
C_D	Sectional drag coefficient
C_x	Sectional force coefficient in the direction of rotation
C_y	Section force coefficient normal to the plane of rotation'
C_p	Power coefficient, $P/(1/2)\rho AV_\infty^3$ or $P/(1/2)\rho SV_\infty^3$
D′	Sectional drag force per unit length
E	Lift to drag ratio, L/D
L′	Sectional lift force per unit length
$\dot{m}$	Mass flow rate
P	Power extracted from the air
p	Pressure
R	Rotor radius
r	Local rotor radius
S	Rotor or translator projected surface area
u	Axial flow velocity at the rotor

u_l Axial flow velocity in the wake

v_∞ Free stream wind velocity

W Resultant velocity relative to the rotor element

X Tip speed ratio, $R\Omega/V_\infty$

x Local speed ratio, $r\Omega/V_\infty$

Greek

α Angle of attack

β Angle between the wind and the normal to the translation velocity, Chapter 2; blade pitch angle, Chapter 5,6.

ϕ Angle between the plane of rotation and the relative velocity

η Wind-height relation exponent

ν Translator velocity

θ Blade pitch angle, Chapters 3, 4; blade rotation angle, Chapters 5, 6

ρ Fluid density

Ω Rotor angular velocity

ω Fluid angular velocity downwind of the rotor

APPENDIX I

WIND TURBINE PERFORMANCE AND LOADS PROGRAM

The program package is written in the Fortran language and utilizes a Simpson's Rule/three pass method of numerical integration. It was written using a CDC 3300 under the OS-3 operating package at Oregon State University, therefore there may be some small differences for implementation on other systems.

Logical unit numbers 60, 61, and 62 in the program refer to the card reader, line printer, and card punch respectively.

The program package consists of a main program with eight subroutines: the main program PROP performs integration, input and output functions; subroutine TITLES prints input listing and titles for output; subroutine SEARCH calculates chord and twist angle at a given station; subroutine CALC determines axial and angular interference factors and related parameters; subroutine TIPLOS calculates the tip loss factor arid the hub-loss factor; subroutine BESSEL calculates modified Bessel functions; subroutines NACA00 determines sectional lift and drag coefficients for NACA profile 0012; subroutine NACA44 determines sectional lift and drag coefficients for NACA profile 4418; NACAXX is an empty subroutine for which a curvefit for any airfoil section can be placed without other program changes.

For a given propeller geometry the following information must be inputted and/or changes made.

1. Subroutine NACAXX must be rewritten to conform to airfoil section used, if other than NACA 4418, and 0012.
2. Blade geometry must be specified, i.e., chord and twist as a function of percent radius.
3. Operating conditions specified.

The parameters to be inputted are:

Radius of blade – R - ft

Hub radius – HB - ft

Incremental Percentage (percent of radius for integration incrementation) – DR

Pitch angle – THETP - degrees

Number of blades – B

Wind velocity – V - mph

Tip speed ratio – X

Axial Interference Model Code – AMOD

$$\begin{cases} 0 - \text{original} \\ 1 - \text{Wilson, seeAppendixII} \end{cases}$$

Altitude above sea level – H - ft

Coning angle – SI - degrees

Number of inputted stations for blade geometry specification – NF

NACA Profile – NPROF - 4418 - NACA 4418
0012 - NACA 0012
9999 - Profile curvefit to be in subroutine NACAXX

Tip loss model controller – GO - 0 - Prandtl
1 – Goldstein
2 - None

Hub loss mode controller – HL - 0 - None
1 - Prandt 1

Percent radius for stations RR (I)

Chord dor stations (CI(I)) - ft

Twist angle for stations – THETI(I) - degrees

Input should be in the following format:

Columns	Card 1	Card 2	Card 3	Card 4	(Card 5 → Card NF)
1-10	R	B	H	HL	RR(I)
11-20	DR	V	81		CI(I)
21-30	HB	X	NF (21-22)		THETI (I)
31-40	THETP	AMOD	GO		
41-50			NPROF		

Output will be printed on the basis of 140 character-field width.

There are several operation controllers that must be -inputted. These are AMOD , GO, HL, and NPROF. AMOD determines which method for calculation of axial and angular interference factors will be used. An input of 0.0 means the Glauert form will also be used, while an input of 1.0 means the square root form will be used. GO determines the tip loss model. An input of 0.0 means Prandtl's model is to be used, the input 1.0 means Goldstein's model is to be used, unless the number of blades is greater than two, then the program will choose Prandtl's model, and an input of 2.0 means no tip loss model is to be used. The third controller is HL; it controls the hub loss model. An input of 0.0 means no hub loss model will be used, while an input of 1.0 means Prandtl's method is to be used. An input of 0012 means subroutine NACA00 is to be used, which is a subroutine that calculates sectional lift and drag data for the NACA profile 0012; an input of 4418 means subroutine NACA44 is to be used to calculate sectional lift and drag data for the NACA profile 4418; an input of 9999 means subroutine NACAXX is to be used. NACAXX is a subroutine one must add a curve fit for sectional lift and drag coefficients as a function of angle of attack (degrees). This enables the user to use other profiles without changes to the program.

The following are the input Read and Format statements used.

```
      READ (60,10) R,DR,HB,THETP
10    FORMAT (4F10.3)

      READ (60,10) B,V,X,AMOD
10    FORMAT (4F10.3)

      READ (60,30) H,SI,NF,GO,NPROF
30    FORMAT (2F10.3,I2,8X,F10.2,I4)

      READ (60,40) HL
40    FORMAT (F10.3)

      READ (60,20) (RR(I),THETI(I),I=l,NF)
20    FORMAT (F5.l,5X,F10.5,Fl0.5)
```

It should also be noted, that the program takes approximately ten seconds to be compiled on the CDC 3300. Therefore, if many runs are desired, it would be desirable to convert the program to binary form.

```
      0S3 FORTRAN  VERSION 3.12          05/17/74  1045

1               PROGRAM PROP
2       C
3       C       ..... MAIN PROGRAM .....
4       C       PROP CALCULATES THE THEORETICAL PERFORMANCE PARAMETERS OF A
5       C       PROPELLER TYPE WIND TURBINE. IT UTILIZES A SIMPSON≠S-RULE
6       C       METHOD / THREE PASS TECHNIQUE OF NUMERICAL INTEGRATION.
7       C
8       C       DIMENSION RR(25),CI(25),THETI(25)
9               COMMON R,DR,HB,B,V,X,THETP,AMOD,H,SI,GO,OMEGA,RHO,VIS,HL,PI,RX,
10             1W,NPROF,T1,T2,T3,T4,T5,T6,T7,58
11      C
12      C       ..... READ INPUT DATA .....
13      C
14              READ(60,10)R,OR,HB,THETP
15              READ(60,10)B,V,X,AMOD
16              READ(60,30)H,SI,NF,GO,NPROF
17              READ(60,40)HL
18              READ(60,20)(RR(I),OI(I) ,THETI(I),I=1,NF)
19              PI=3.1415926S36
20              OMEGA=V*X/R*2640./(60.*PI)
21      C
22      C       ..... PRINT INPUT AND TITLES FOR OUTPUT .....
23      C
24      C       CALL TITLES(RR,CI,THETI,NF)
25      C
26      C       ..... INITIALIZATION AND CONSTANT PARAMETER CALCULATIONS .....
27      C
28              ITOT=0
29              T1=0.0
30              T2=0.0
31              T3=0.0
32              T4=0.0
33              T5=0.0
34              T6=0.0
35              T7=0.0
36              T8=0.0
37              QY=0.0
38              TY=0.0
39              PY=0.0
40              QX=0.0
41              TX=0.0
42              XMXY=0.0
43              XMYY=0.0
44              XMXX=0.0
45              XMYX=0.0
46              ASTOP=0.0
47              A=.05
48              V=V*5280./3600.
49              SI=SI*PI/180.
50              THETP=THETP*PI/180.
51              ALPLO=ALPLO*PI/180.
52              RHO=0.0023769199*EXP(-0.297*H/10000.)
53              VIS=0.0000003719 - 0.00000000204*H/1000.
54              OMEGA=V*X/R
55              NN=(R-HB)/DR +1.
56              RX=R
57              RLB=(1,-DR)*RX
58              DR=(RX-RLB)*COS(SI)
59              R=R*COS(SI)
```

```
60              HB=HB*COS(SI)
61              RL=R
62      C
63      C       ..... THREE PASS - NUMERICAL INTEGRATION FROM TIP TO HUB .....
64      C
65              DO 100 L=1,NN
66              IF((RL-HB).GE.DR)GO TO 50
67              ASTOP=ASTOP+1.
68              IF(ASTOP.GE.2.) GO TO 93
69              DR=(RL-HB)
70      50      DR2=DR/2.
71              DT6=DR/6.
72              RL-RL-DR2
73              AK=1.
74              CALL SEARCH(RL,RR,CI,THETI,NF,O,THET)
75              CALL CALC(RL,C,THET,FXXP1,FYXP1,XMXXP1,XMYXP1,QXP1,TXP1,RE,
76             1PHIR,CL,CD,CX,CY,A,AP,XL,AK,ALPHA,F)
77              RL=RL-DR2
78              AK=0.0
79              CALL SEARCH(RL,RR,CI,THETI,NF,C,THET)
80              CALL CALC(RL,C,THET,FXY,FYY,XMXXP,XMYXP,QXP,TXP,RE,PHRI,CL,
81             1CD,CX,CY,A,AP,XL,AK,ALPHA,F)
82              QYX=DT6*(QX+4.*QXP1+QXP)
83              QY=QY + QYX
84              TY=TX+DT6*(TX+4.*TXP1+TXP)
85              PY=PY+OMEGA*QYX
86              XMXY=XMXY+DT6*(XMXX+4.*XMXXP1+XMXXP)
87              XMYY=XMYY+DT6*(XMYX+4.*XMYXP1+XMYXP)
88              QX=QXP
89              TX=TXP
90              XMXX=XMXXP
91              XMYX=XMYXP
92              CTY=TY/(.5*RHO*V**2*PI*RX**2)
93              CPY=PY/(.5*RHO*V**3*PI*RX**2)
94              TP=PY/737.6
95              PHIO=PHIR*180./PI
96              ALPHA=ALPHA*180./PI
97              PR=RL/(RX*COS(SI))
98      C
99      C       ..... PRINT OUTPUT .....
100     C
101             ITOT=ITOT+1
102             IF(ITOT.EQ.4) GO TO 43
103             GO TO 44
104     43      WRITE(61,95)
105             WRITE(61,70)
106             WRITE(61,58)
107             WRITE(61,59)
108             WRITE(61,95)
109             ITOT=0
110     44      CONTINUE
111             WRITE(61,201)RL,PR,F,ALPHA,CL,CD,CX,CY,FXY,FYY,XMXY
112             WRITE(61,200)XMYY,W,QY,CTY,TY,CPY,TP,PHIO,RE
113     100     CONTINUE
114     93      FYKDE=RX/V*T1/PI
115             FYKDG=-T2/PI
116             XMCKDE=-RX/V*T3/PI
117             XMCKDG=T4/PI
118             XMZKDE=RX/V*T3/PI
```

```
119           XMZKDG=-T4/PI
120           CQKDE=-RX/V*T5/PI
121           CQKDG=T6/PI
122           PISTEL=T7/(PI*RX**5)
123           PI2STEL=T8*X/(PI*RX**6)
124           WRITE(61,800)FYKDE
125           WRITE(61,801)FYKDG
126           WRITE(61,802)XMCKDE
127           WRITE(61,803)XMCKDG
128           WRITE(61,804)XMZKDE
129           WRITE(61,80S)XMZKDG
130           WRITE(61,806)CQKDE
131           WRITE(61,807)CQKDG
132           WRITE(61,808)PISTEL
133           WRITE(61,809)PI2STEL
134     C
135     C     ..... FORMATS FOR INPUT AND OUTPUT STATEMENTS .....
136     C
137     10    FORMAT(4F10.3)
138     20    FORMAT(F5.1,5X,F10.5,F10.5)
139     30    FORMAT(2F10.3,I2,8X,F10.2,I4)
140     40    FORMAT(F10.3)
141     95    FORMAT(//≠ XXXXXXXXXXXXXXXXXXXXXXXXXXXXXXXXXXXXXXXXXXXXXXXXXXXXXXXX
142           1XXXXXXXXXXXXXXXXXXXXXXXXXXXXXXXXXXXXXXXXXXXXXXXXXXXXXXXXXXXXXXX≠)
143     70    FORMAT(///9X,≠A≠,14X,≠AP≠,26X,≠FT≠,18X,≠FN≠)
144     58    FORMAT(///LX,≠R≠,10X,≠PC-R≠,8X,≠F≠,7X,≠ALPHA≠,9X,≠CL≠,9X,≠CD≠,9X,≠
145           10X≠,9X,≠CY≠,9X,≠FX≠,8X,≠FY≠,12X,≠MX≠)
146     59    FORMAT(//6X,≠MY≠,16X,≠W≠,15X,≠O≠,11X,≠CT≠,13X,≠T≠,9X,≠CP≠,13X,
147           1≠P≠,9X,≠PHI≠,10X,≠RL NU≠)
148     201   FORMAT(///F7.2,5X,F6.4,5X,F6.4,5X,F7.4,5X,F6.4,5X,F6.4,5X,F6.4,5X,
149           1F5.3,5X,F7.2,5X,F7.2,5X,F11.2)
150     200   FOR1AT(//F11.2,5X,F11.2,5X,F11.2,5X,F6.4,5X,F11.2,5X,F6.4,5X,F10.3
151           1,5X,F6.2,5X,E12.3///)
152     800   FORMAT(/≠(YAW FORCES DUE TO CONING / BLADE) / (SIN(THETK) =≠,
153           1F10.4)
154     801   FORMAT(/≠(YAW FORCES DUE T0 SHEAR / BLADE) / (SIN(THETK)**2) =≠,
155           1F10.4)
156     802   F0RMAT(/≠(CONING M0MENT DUE TO FLAPPING / BLADE) =≠,F10.4)
157     803   FORMAT(/≠(CONING MOMENT DUE TO SHEAR / BLADE) / (SIN(THETK)) =≠,
158           1F10.4)
159     804   FORMAT(/≠(YAWING MOMENT DUE TO FLAPPING / BLADE) / (COS (THETK) =≠,
160           1F10.4)
161     805   FORMAT(/≠(YAWING M0MENT DUE TO SHEAR / BLADE) / (SIN(THETK)*C0S(THE
162           1TK)) =≠F10.4)
163     806   FORMAT(/≠(TORQUE VARIATION DUE TO CONING / BLADE) =≠,
164           1F10.4)
165     807   FORMAT(/≠(T0RQUE VARIATION DUE TO SHEAR / BLADE) / (SIN(THETK)) =≠
166           1,F10.4)
167     808   FORMAT(/≠ T0RQUE VARIATION DUE TO AERODYNAMIC SECOND DERIVATIVE =
168           1 ≠,F15.4)
169     809   FORMAT(/≠ TOROUE VARIATION DUE TO SHEAR SECONO DERIVATIVE = ≠
170           1,F15.4)
171     C
172           STOP
173           END
```

```
174           SUBROUTIE TITLES(RR,CI,THETI,NF)
175     C
176     C     ..... TITLES - PRINTS OUT INPUT DATA IN A DESCRIPTIVE
177     C     FORM, AND PRINTS DESCRIPTIONS OF SYMBOLS/TITLES FOR OUTPUT.
178     C
179           DIMENSION RR(25),CI(25),THETI(25)
180           COMMON R,DR,HB,B,V,X,THETP,AMOO,H,SI,GO,OMEGA,RHO,VIS,HL,PI,RX
181          1,W,NPROF
182           WRITE(61,50)
183           WRITE(61,51)
184           WRITE(61,52) R,DR,HB,THETP
185           WRITE(61,53)B,V,X
186           WRITE(61,54) H,SI,NF
187           WRITE(61,200)OMEGA,NPROF
188           IF(AMOD.EQ.0.0) GO TO 300
189           WRITE(61,310)
190           GO TO 340
191     300   WRITE(61,320)
192     340   IF(B.GT.2.0) GO TO 655
193           IF(GO.EQ.0.0) GO TO 103
194           IF(G0.EQ 1.0) GO T0 656
195           IF(GO.EQ.2.0) GO TO 657
196           GO TO 658
197     655   IF(GO.EQ.2.0) GO TO 657
198           GO TO 103
199     656   WRITE(61,101)
200           G0 T0 658
201     657   WRITE(61,659)
202           GO TO 658
203     103   WRITE(61,100)
204     658   IF(HL.EQ.0.0) GO TO 777
205           WRITE(61,778)
206
207           GO TO 666
208     777   WRITE(61,779)
209     666   WRITE(61,55)
210           WRITE(61,56)(RR(I),CI(I),THETI(I),I=1,NF)
211           WRITE(61,57)
212           WRITE(61,61)
213           WRITE(61,169)
214           WRITE(61,71)
215           WR1TE(61,60)
216           WRITE(61,62)
217           WRITE(61,63)
218           WRITE(61,64)
219           WRITE(61,65)
220           WRITE(61,66)
221           WRITE(61,67)
222           WRITE(61,68)
223           WRITE(61,69)
224           WRITE(61,95)
225           WRITE(61,70)
226           WRITE(61,58)
227           WRITE(61,59)
228           WRITE(61,95)
229     C
230     C     ..... FORMATS FOR OUTPUT STATEMENTS .....
231     C
232     50    FORMAT(////≠ THEORETICAL PERFORMANCE OF A PROPELLER TYPE WIND TURB
```

```
      0S3 FORTRAN  VERSION 3.12 TITLES  05/17/74  1045

233           1INE≠)
234     51     FORMAT(///≠ DATA INPUT RECORD ≠)
235     52     FORMAT(///≠ RADIUS-FT=≠,F7.2,10X,≠INCREMENTAL PERCENTAGE =≠,F6.4,
236           110X,≠HUB RADIUS-FT=≠,F5.2,10X,≠PITCH ANGLE - DEGREES =≠,F7.4)
237     53     FORMAT(/≠ NO. OF BLADES =≠,F3.0,10X,≠WIND VELOCITY - MPH =≠,F7.2,
238           110X,≠TIP SPEED RATIO =≠,F6.3)
239     54     FORMAT(//≠ ALTITUDE OF SITE ABOVE SEA LEVEL-FT=≠,F10.2,5X,≠CONING
240           1ANGLE-DEGREES =≠,F7.3,5X,≠NUMBER OF DATA STATIONS ALONG SPAN =≠,I2
241           1)
242     55     FORMAT(///≠ PERCENT RADIUS≠,5X,≠CHORD-FT≠,5X,≠TWIST ANGLE-DEGREES≠
243           1)
244     56     FORMAT(//5X,F5.1,8X,F10.5,10X,F10.5)
245     57     FORMAT(///////≠ DATA OUTPUT RECORD≠////)
246     60     FORMAT(≠ RADIUS -- FT -- R≠/≠ PERCENT RADIUS -- PC-R≠)
247     61     FORMAT(≠ AXIAL INTERFERENCE FACTOR -- A≠/≠ ANGULAR INTERFERENCE FA
248           1CTOR -- AP≠)
249     169    F0RMAT(≠ NORMAL FORCE -- FN≠/≠ TANGENTIAL FORCE --FT≠)
250     62     FORM4T(≠ LIFT COEFFICIENT -- CL≠/≠ DRAG COEFFICIENT -- CO≠)
251     63     FORMAT(≠ C0EF OF FOKCE-X-DIR -- CX≠/≠ COEF OF FORCE-Y-DIR -- CY≠)
252     64     FORMAT(≠ FORCE-X-DIR/BLAOE -- LB -- FX≠/≠ FORCE-Y-DIR/BLADE – LB
253           1--FY≠)
254     65     FORMAT(≠ MOMENT-X-DIR/BLADE -- FT-LB -- MX≠/≠ MOMENT-Y-DIR/BLAOE
255           1-- FT-LB -- MY≠)
256     66     FORMAT(≠ RELATIVEC VELOCITY -- FT/SEC --W≠/≠ TORQUE -- FT-LB -- Q≠)
257     67     FORMAT(≠ THRUST COEFFICIENT -- CT≠/≠ THRUST -- LB --T≠)
258     68     FORMAT(≠ POWER COEFFICIENT -- CP≠≠ POWER -- KILOWATTS -- P≠)
259     69     FORMAT(≠ ANGLE PHI -- DEGREES -- PHI ≠/≠ REYNOLDS NUMBER -- RE NO≠)
260     71     FORMAT(≠ TIP LOSS FACTOR -- F≠/≠ ANGLE OF ATTACK -- DEGREES – ALP
261           1HA≠)
262     95     FORMAT(//≠ XXXXXXXXXXXXXXXXXXXXXXXXXXXXXXXXXXXXXXXXXXXXXXXXXXXXXXXX
263           1XXXXXXXXXXXXXXXXXXXXXXXXXXXXXXXXXXXXXXXXXXXXXXXXXXXXXXX~XXXXXXXXX≠)
264     70     FORMAT(///9X,≠A≠,14X,≠AP≠,26X,≠FT≠,18X,≠FN≠)
265     58     FORMAT(///4X,≠R≠,10X,≠PC-R≠,8X,≠F≠,7X,≠ALPHA≠,9X,≠CL≠,9X,≠CD≠,9X,≠
266           1CX≠,9X,≠CY≠,9X,≠FX≠,8X,≠FY≠,12X,≠MX≠)
267     59     F0RMAT(//6X,≠MY≠,16X,≠W≠,15X,≠Q≠,11X,≠CT≠,13X,≠T≠,9X,≠CP≠,13X,
268           1≠P≠,9X,≠PHI≠,10X,≠RE NO≠)
269     310    FORMAT(//≠ WILSON AXIAL INTERFERENCE METHOD USED≠)
270     320    FORMAT(//≠ STANOARO AXIAL INTERFERENCE METHOD USED≠)
271     100    FORMAT(//≠ TIP LOSSES MODELED BY PRANDTLS FORMULA ≠)
272     101    FORMAT(//≠ TIP LOSSES MODELED BY GOLDSTEINS FORMULA ≠)
273     659    FORMAT(//≠ NO TIP LOSS MODEL USED≠)
274     778    FORMAT(//≠ HUBLOSSES MODELED BY PRANDTL≠)
275     779    FORMAT(//≠ NO HUBLOSS MODEL USED≠)
276     200    FORMAT(//≠ RPM = ≠,F20.5,10X,≠NACA PROFILE =≠,I4)
277     C
278           RETURN
279           END
```

```
      OS3 FORTRAN  VERSION 3.12          05/17/74  1045

280           SUBROUTINE SEARCH(RL,RR,CI,THETI,NF,O,THET)
281     C
282     C     ..... SEARCH - DETERMINES THE CHORD AND THE TWIST ANGLE AT
283     C     A GIVEN RADIUS ALONG THE SPAN. IT UTILIZES A LINEAR
284     C     INTERPOLATION TECHNIQUE.
285     C
286           DIMENSION RR(25),CI(25),THETI(25)
287           COMMON R,DR,HB,B,V,X,THETP,AMOD,H,SI,GO,OMEGA,RHO,VIS,HL,PI,RX
288           DO 20 1=1,NF
289           RRV=RL/(RX*COS(SI))*100.
290           IF(RRV.GE.RR(*I)) GO TO 10
291           IF(I.EQ.NF) GO TO 30
292     20    CONTINUE
293     10    J=I+1
294           PER=(RRV-RR(J-100/(RR(J-2)-RR(J-1))
295           C=PER*(CI(J-2)-CI(J-1))+CI(J-1)
296           THET=PER*(THETI(J-2)-THETI(J-1))+THETI(J-1)
297           GO TO 40
298     30    C=CI(NF)
299           THET=THETI(NF)
300     40    THET=THET*PI/180.
301           RETURN
302           END
```

```
      0S3 FORTRAN  VERSION 3.12          05/17/74  1045

202           SUBROUTINE CALC(RL,C,THET,FXF,FYF,XMFXF,XMFYF,QF,TF,RE,PHIR,CL,
304          1CD,CX,CY,A,AP,XL,AK,ALPHA,F)
305     C
306     C     ..... CALC - DETERMINES THE AXIAL AND ANGULAR INTERFERENCE
307     C     FACTORS AT A GIVEN RADIUS AND DETERMINES FUNCTIONS DEPENDENT
308     C     UPON THESE PARAMETERS.
309     C
310           COMMON R,DR,HB,B,V,X,THETP,AMOD,H,SI,GO,OMEGA,RHO,VIS,HL,PI,RX
311          1W,NPROF,T1,T2,T3,T4,T5,T6,T7,T8
312           XL=RL*OMEGA/V
313           RH=HB
314           DO 10 J-1,40
315           BETA=A
316           DELTA=AP
317           PHI=ATAN((1.-A)*COS(SI)/((1.+AF)*XL))
318           PHIAA=ABS(PHI)
319           XXL=COS(PHIAA)/SIN(PHIAA)
320           XXLO=XXL*R/RL
321           PHIR=FHI
322           ALPHA=PHI-THET-THETP
323           ALPHAD=ALPHA+0.001
324     C
325     C     ..... CALCULATION OF SECTIONAL LIFT AND DRAG COEFFICIENTS
326     C
327           IF(NPROF.EQ.4418) GO TO 400
328           IF(NPROF.EQ.0012) GO TO 500
329           IF(NPROF.EQ.9999) GO TO 550
330           WRITE(61,600)
331     600   FORMAT(≠ YOU HAVE SPECIFIED A NACA PROFILE NOT STORED IN THE PROGR
332          1AM, THE PROGRAM WILL USE NACA 4418.≠)
333     400   CALL NACA44(ALPHA,CL,CD)
334           CALL NACA44(ALPHAD,CLD,CDD)
335           GO T0 800
336     500   CALL NACA00(ALPHA,CL,CD)
337           CALL NACA00(ALPHAD,CLD,CDD)
338           GO TO 800
339     550   CALL NACAXX(RL,RX,SI,ALPHA,CL,CD)
340           CALL NACAXX(RL,RX,SI,ALPHAD,CLD,CDD)
341     800   IF(ABS(ALPHA).GE.(2.*PI/12.)) CL=0.0
342     C
343     C     ..... CALCULATION OF TIP AND HUB LOSSES .....
344     C
345           CALL TIPLOS(XXL,XXLO,F,B,GO,HL,PI,R,RL,PHI,RH)
346     C
347           CX=CL*SIN(PHI)-CD*COS(PHI)
348           CY= CL*COS(PHI)*COS(SI)+CD.SIN(PHI)*COS(SI)
349           SIG=(B*C)/(PI*RL)
350           IF(AMCD.EQ.0.) GO TO 575
351           VBR=(0.12S*SIG*CY)/(SIN(PHI)**2)
352           VAR=(0.125*SIG*CX)/(F*SIN(PHI)*COS(PHI))
353           CAN=F*F+4.*VBR*F*(1.-F)
354           IF(CAN.LT.0.0) CAN=0.0
355           A=(2.*VBR.F-SQRT(CAN))/(2.*(VBR+F*F))
356           AP=VAR/(1.-VAR)
357           GO TO 580
358     575   VBR=0.125*SIG*CY
359           VAR=0.125*SIG*CX
360           A=VBR/(F*SIN(PHI)**2+VVR)
361           AP=VAF/(F*SIN(PHI)*COS(PHI)-VAR)
```

```
362     580     PCR=RL/(RX*COS(SI))
363     C       ..... DAMPENING OF AXIAL AND ANGULAR INTERFERENCE FACTOR
364             ITERATIONS.
365     C
366             IF(J-4) 30,40,90
367             IF(J-10)  30,40,110
368     110     IF(J-15) 30,40,30
369     40      A=(A+BETA)*.5
370             AP=(AP+DELTA)*.5
371     C
372     30      IF(AK.GE.1.) GO TO 70
373             WRITE(61,60) A, AP
374     60      FORMAT(2F15.8)
375     C
376     C       ..... TEST FOR CONVERGENCE .....
377     C
378     70      IF(ABS((AP-DELTA)/AP).LE..0001) GO TO 50
379     C
380     10      CONTINUE
381     C
382     C       ..... CALCULATION 0F FUNCTIONS DEPENDENT UP0N AXIAL AND
383     C       ANGULARINTERFERENCE FACTORS.
384     C
385     50      W=((1.-A)*V*COS(SI))/(SIN(PHI))
386             RE=RHO*W*C/VIS
387             CONST=(0.5*RHO*(W**2)*C)
388             FXF=CONST*CX
389             FYF=CONST*CY
390             XMFXF=FXF*(RL-HB)
391             XMFYF~FYF*(RL-HB)
392             CT1=(0.5*RHO*B*C)*(W*W)
393             QF=CT1*RL*CX
394             TF=CT1*CY
395             DPCR=DR/(2.*RX)
396             CR=C/RX
397             CLA=(CLD-CL)/0.001
398             CDA=(CDD-CD)/0.001
399             CXP=CLA*SIN(PHI)-CDA*COS(PHI)+CY
400             CYP=CLA*COS(PHI)+CDA*SIN(PHI)-CX
401             FT=(2.*CX+CXP/ATANF(PHI))*(1.-A)*CR*PCR
402             FN=(2.*CY+CYP/ATANF(PHI))*(1.-A)*CR*PCR
403             WRITE(61,699) FT,FN
404     699     FORMAT(40X,2F20.7)
405             T1=T1+FT*DPCR
406             T2=T2+FT*(1.-A)DPCR
4O7             T3=T3+FN*PCR*DPCR
408             T4=T4+FN*(1.-A)*PCR*DPCR
409             T5=T5+FT*PCR*DPCR
410             T6=T6+FT*(1,-A)*PCR*DPCR
411             T7=T7+(((2.-COS(PHI)**2)*CL*SIN(PHI)-2.*COS(PHI)**3*CD+
412            12.COS(PHI)*CLA)*(1.-A)**2*RL**3*C)*DR/2.
413             T8=T8+(((1.+SIN(PHI)**2)*CL-CO*SIN(PHI)+CLA*SIN(PHI))
414            1*(1.+AP)*(1.-A)*RL*4*C)*DR/2.
415     C
416             RETURN
417             END
```

```
418
419           SUBROUTINE TIPLOS(U,UO,F,Q,GO,HL,PI,R,RL,PHI,RH)
420     C
421     C     ..... TIPLOS - DETERMINES THE TIP AND HUB LOSSES
422           BASED UPON GOLDSTEIN≠S THEORY, OR PRANDTL≠S THEORY,
423           OR FOR THE CASE OF NO LOSSES.
424     C
425           SUM2=0.0
426           SUM=0.0
427           AK=1.
428           AMM=1.
429           AM=0.0
430           IF(O.GT.2.0) GO TO 966
431           IF(GO.EQ.0.0) GO TO 200
432           IF(GO.EQ.1.0) GO TO 100
433           IF(GO.EQ.2.0) GO T0 444
434     966   IF(GO.EQ.2.0) GO TO 444
435     200   CONTINUE
436           F=(2./PI)*ACOSF(EXP(-(Q*(R-RL))/(2.*RL*SQRT(SIN(PHI)**2 +.0001))))
437           GO TO 105
438     444   F=1.0
439           GO TO 105
440     100   IF((ABS(SIN(PHI))).LT..0001) GO TO 200
441     C
442     C     .... GOLDSTEINS METHOD.....
443     C
444           DO 10 M=1,3
445           V=(2.*AM+1.)
446           Z0=UO*V
447           V2=V*V
448           Z=U*V
449           Z2=Z*Z
450           CALL BESSEL(Z,V,AI)
451           CALL BESSEL(Z0,V,AI0)
452           IF(Z.GE.3.5) GO TO 300
453           A=2.*2.
454           B=4.*4.
455           C=6.*6.
456           D=8.*8.
457           TIVZ=Z2/(A-V2)+(Z2*Z2)/((A-V2)*(B-V2))+(Z2**3)/((A-V2)*(B-V2)*
458          1(C-V2))+(Z2**4)/((A-V2)*(B-V2)*(C-V2)*(D-V2))
459           CT1VZ=(V*PI*AI)/(2.*SIN(.5*V*PI)) -T1VZ
460           GO TO 400
461     300   T0=(U*U)/(1.+U*U)
462           T2=4.*U*U*((1.+U*U)**4
463           T4=16.*U*U*(1.-14.*U*U+21.*U**4 - 4.*U**6)/((1.+U*U)**7)
464           T6=64.*U*U*(1.-75.*U*U+603.*U**4-1065.*U**6+460.*U**8-36.*U**10)
465          1/((1.+U*U)**10)
466           CT1VZ=T0+T2/V2+T4/(V2**2)+T6/(V2**3)
467     400   FVU=(U*U)/(1.+U*U) - CT1VZ
468           SUM=SUM+FVU/V2
469           IF(AM.NE.0.0) GO TO 1
470           E=-0.098/(UO**.668)
471     1     IF(AM.NE.1.0) GO TO 2
472           E=0.031/(UO**1.285)
473     2     IF(AM.GT.1.0) E=0.0
474           SUM2=SUM2+((UO*UO*AMM)/(1.+UO*UO) -E)*(AI/AIO)
475           AM=AM+1.
476           AK=((2.*AM-1.)*AK)/(2.*AM)
```

```
      0S3 FORTRAN  VERSION 3.12 TIPLOS  05/17/74  1045

477   10      AMM=AK/(2.*AM+1.)
478           G=(U*U)/(1.+U*U)-(8./(PI*PI))*SUM
479           CIRC=G-(2./PI)*SUM2
480           F=((1.+U*U)/(U*U))*CIRC
481   C
482   C       HUBLOSS CALCULATIONS
483   C
484   105     IF(HL.EQ.1.0) GO TO 500
485           FI=1.0
486           GO TO 900
487   500     FI=(2./PI)*ACOSF(EXP(-(Q*(RL-RH))/(2.*RH*SQRT(SIN(PHI)**2+
488          1.0001))))
489   900     F=F*FI
490           RETURN
491           END
```

```
      0S3 FORTRAN  VERSION 3.12          05/17/74  1045

492           SUBROUTINE BESSEL(Z,V,AI)
493   C
494   C       ..... BESSEL CALCULATES BESSEL FUNCTIONS FOR THE GOLDSTEIN
495           TIP LOSS MODEL.....
496   C
497           S=0.0
498           AK=0.0
499           C= 1.
500           DO 30 K=1,10
501           B=(.25*Z*Z)**AK
502           D=V+AK
503           P=1.
504   5       TK=D-1.
505           IF(TK.LE.0.0) GO TO 40
506           P=D*TK*P
507           D=D-2.
508           GO TO 5
509   40      E=P
510           S=B/(C*E) + S
511           AK=AK+1.
512           C=AK*C
513   30      CONTINUE
514           AI=((.5*Z)**V)*S
515           RETURN
516           END
```

```
      0S3 FORTRAN  VERSION 3.12          05/17/74  1045

517           SU8ROUTINE NACA00(ALPHA,CL,CD)
518   C
519   C       ..... NACA - DETERMINES THE C0EFFICIENTS 0F LIFT AND DRAG
520   C       AT A GIVEN ANGLE 0F ATTACK, ALPHA; FOR A NACA 0012 AIRF0IL.
521   C       THE EQUATIONS WERE 0BTAINED BY A ORTHOGNAL P0LYNOMIAL
522   C       CURVEFIT OF NACA DATA PUBLISHED IN NACA REPORT NO. 669,PAGE 529.
523   C
524           A0=5.73
525           A2=7.*A0
526           SD0=0.0058
527           SD1-0.0006
528           SD2=.130
529           SD3=0.0168
530           SD4=0.0006
531           SD5=12570.
532           AMAX=0.218
533           A=ALPHA
534           IF(A.GT.AMAX) GO TO 24
535           CL=A0*A
536           CD=SD0+(SD1+A)+(SD2*A*A)
537           GO T0 25
538           CL=(A0*A)-(A2*(A-AMAX)**2)
539           IF(CL.GE.0.0) GO TO 61
540           CL=0.0
541           CD=SD3+SD4*(A-AMAX)**2 +SD5*(A-AMAX)**4
542           IF(CD.LE.1.0) G0 TO 25
543           CD=1.0
544   25      RETURN
545           END
```

```
546             SUBROUTINE NACA44 (ALPHA,CL,CD)
547     C
548     C       ..... NACA - DETERMINES THE COEFFICIENTS OF LIFT AND DRAG
549     C       AT A GIVEN ANGLE OF ATTACK, ALFHA; FOR A NACA 4418 AIRFOIL.
550     C       THE EQUATIONS WERE OBTAINED BY A ORTHOGNAL POLYNOMIAL
551     C       CURVEFIT OF NACA DATA PUBLISHED IN NACA REPORT NO. 824, PAGE 401.
552     C
553             ALP=ALPHA*180./3.141593
554             IF(ALP.GE.8.0) GO TO 20
555             CL=0.099375*ALP + 0.3975
556             IF(ALF.6G.+2.0) GO TO 10
557             CD=0.00001644&ALP + 0.000028188623*ALP**2 - 0.000000704*ALP**3
558            1+0.00661
559             GO TO 100
560     10      CD=0.0001695356*ALP + 0.00002732*ALP**2 + 0.0000023229*ALP**3
561            1+ 0.00629752
562             GO TO 100
563     20      IF(ALP.GE.12.0) GO TO 30
564             CL= 0.0731*ALP + 0.6078
565             GO TO 10
566     30      IF(ALP. GE.15.5) GO T0 50
567             CL= 0.214377*ALP - 0.00738*ALP**2 - 0.0248
568             GO TO 10
569     50      IF(ALP.GE,16.0) GO TO 60
570             CL= -0.11*ALP + 3.23
571             GO TO 10
572     60      CL= -0.029*ALP +1.934
573             CD=+0.0131686686494*ALF - 0.1851985
574     100     RETURN
575             END
```

```
      0S3 FORTRAN  VERSION 3.12          05/17/74  1045

576           SUBROUTINE NACAXX(ALPHA,CL,CD)
577     C
578     C     ..... NACAXX IS AN EMPTY SUBROUTINE FOR USE FOR A PROFILE
579     C     NOT PREVIOUSLY STORED. ONE MUST INSERT CURVE FIT EQUATICNS
580     C     FOR SCCTIONAL LIFT AND DRAG COEFFICIENTS AS A FUNCTION OF
581     C     ANGLE OF ATTACK IN DEGREES.
582     C
583           ALP=ALPHA*188./3.141593
584     C     ADD CURVE FIT PROGRAM FOR CL AND CD
585           RETURN
597           END


NO ERRORS FOR NACAXX
LENGTH OF SUBPROGRAM.     00026
```

APPENDIX II

THE USE OF THE "F" FACTORS

Since vorticity is conserved, the circulation in the wake must be equal to the circulation "generated" by the blades

Hence

$$\Gamma_{total} = \oint \vec{v} \cdot \vec{ds}$$

Using a circular path

$$\Gamma_{total} = \int_0^{2\pi} \{2a'r\Omega\} r d\theta$$

↑
wake
tangent
velocity

For an infinite number of blades $a' \neq a'(\theta)$, i.e., a' is constant.

$$\Gamma_{total_{B\to\infty}} = 4\pi r\, a'r\Omega$$

For finite blades a' is a function of θ, increasing near the blades and decreasing in between.

Hence, the circulation Γ is a function of the circulation calculated above

$$\Gamma_{total} = \frac{4\pi r F\, a'r\Omega}{B} \text{ per blade}$$

At this same time, from Kutta-Joukowski

$$\Gamma_{lift} = \frac{c}{2} C_L\, W$$

Now Γ_{total} included the drag generated circulation the ratio of Γ_{total} to Γ_L is

$$\frac{\Gamma_T}{\Gamma_L} = \frac{C_x}{C_L \sin\phi}$$

Since $d\vec{Q}_x = \left(\vec{r}x d\vec{F}\right)_x$

$$d\vec{F} = \rho \vec{W} x \vec{\Gamma} dr \ , \ dF_x = \tfrac{1}{2}\rho W^2 \, c C_x dr$$

Combining

$$\frac{C_x}{C_L \sin\phi} = \frac{4\pi r F \, a' r\Omega}{Bc \, C_L W} \ , \ \frac{r\Omega}{W} = \frac{\cos\phi}{1+a'}$$

since $\sigma \equiv \dfrac{Bc}{\pi r}$

$$\frac{1}{1+a'} = \frac{\sigma C_x}{8F \sin\phi \cos\phi}$$

Now thrust is determined by

$$dT_{momentum} = dT_{blade\ element}$$

$$\rho V_\infty (1-a) 2a V_\infty 2\pi r dr = \frac{B}{2} \rho W^2 C_y c dr$$

Consider "a" to be localized at the rotor disk also, then

$$(1-aF)aF = \frac{\sigma C_y}{8\sin^2\phi}(1-a)^2 \equiv S(1-a)^2$$

$$a = \frac{2S = F - \sqrt{F^2 + 4SF(1-F)}}{2(S+F^2)}$$